International Journal of Pharmaceutics 657 (2024) 124187

Contents lists available at ScienceDirect

International Journal of Pharmaceutics

journal homepage: www.elsevier.com/locate/ijpharm

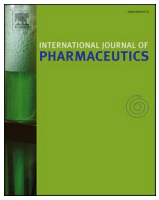

Cyclodextrin encapsulation enabling the anticancer repositioning of disulfiram: Preparation, analytical and *in vitro* biological characterization of the inclusion complexes

Beáta-Mária Benkő [a], Gergő Tóth [b], Dorottya Moldvai [c], Szabina Kádár [b,d], Edina Szabó [d], Zoltán-István Szabó [e], Márta Kraszni [b], Lajos Szente [f], Béla Fiser [g,h,i], Anna Sebestyén [c], Romána Zelkó [a,*], István Sebe [a,j]

[a] *University Pharmacy Department of Pharmacy Administration, Semmelweis University, Hőgyes Endre Str. 7-9., Budapest 1092, Hungary*
[b] *Department of Pharmaceutical Chemistry, Semmelweis University, Hőgyes Endre Str. 7-9., Budapest 1092, Hungary*
[c] *Tumor Biology, Cell and Tissue Culture Laboratory, 1st Department of Pathology and Experimental Cancer Research, Semmelweis University, Üllői út 26., Budapest 1085, Hungary*
[d] *Department of Organic Chemistry and Technology, Faculty of Chemical Technology and Biotechnology, Budapest University of Technology and Economics, Műegyetem rkp. 3., Budapest 1111, Hungary*
[e] *Faculty of Pharmacy Department of Drugs Industry and Pharmaceutical Management, George Emil Palade University of Medicine, Pharmacy, Science and Technology of Targu Mures, Gheorghe Marinescu Str. 38, Târgu Mureș 540142, Romania*
[f] *CycloLab Cyclodextrin Research & Development Laboratory Ltd., Illatos út 7, Budapest 1097, Hungary*
[g] *Institute of Chemistry, Faculty of Materials Science and Chemical Engineering, University of Miskolc, Egyetemváros, Miskolc 3515, Hungary*
[h] *Department of Physical Chemistry, Faculty of Chemistry, University of Lodz, 90-236 Lodz, Poland*
[i] *Ferenc Rakoczi II Transcarpathian Hungarian College of Higher Education, 90200 Beregszász, Transcarpathia, Ukraine*
[j] *Egis Pharmaceuticals Plc., R&D Directorate, P.O. Box 100, Budapest 1475, Hungary*

A R T I C L E I N F O

Keywords:
Disulfiram
Cyclodextrin
Anticancer
Repositioning
Glioblastoma
Melanoma

A B S T R A C T

Drug repositioning is a high-priority and feasible strategy in the field of oncology research, where the unmet medical needs are continuously unbalanced. Disulfiram is a potential non-chemotherapeutic, adjuvant anticancer agent. However, the clinical translation is limited by the drug's poor bioavailability. Therefore, the molecular encapsulation of disulfiram with cyclodextrins is evaluated to enhance the solubility and stability of the drug. The present work describes for the first time the complexation of disulfiram with randomly methylated-β-cyclodextrin. A parallel analytical and in vitro biological comparison of disulfiram inclusion complexes with hydroxypropyl-β-cyclodextrin, randomly methylated-β-cyclodextrin and sulfobutylether-β-cyclodextrin is conducted. A significant drug solubility enhancement by about 1000-folds and fast dissolution in 1 min is demonstrated. The in vitro dissolution-permeation studies and proliferation assays demonstrate the solubility-dependent efficacy of the drug. Throughout the different cancer cell lines' characteristics and disulfiram unspecific antitumoral activity, the inhibitory efficacy of the cyclodextrin encapsulated drug on melanoma (IC_{50} about 100 nM) and on glioblastoma (IC_{50} about 7000 nM) cell lines differ by a magnitude. This pre-formulation

Abbreviations: AB, Alamar Blue assays; ALDH, aldehyde dehydrogenase; ATR-FTIR, Attenuated total reflectance Fourier-Transform infrared spectroscopy; 2D ROESY, two-dimensional phase-sensitive rotating-frame Overhauser effect spectroscopy; BCS, biopharmaceutical classification system; CD, cyclodextrin; CE, complexation efficiency; CZE, capillary zone electrophoresis; DEDTC, diethyldithiocarbamate; DF, degrees of freedom; DIS, disulfiram; DS, degrees of substitution; DSC, differential scanning calorimetry; GB, glioblastoma; G, guest; H, host; HPBCD, hydroxypropyl-β-cyclodextrin; J(t), flux; K_{stab}, equilibrium constant; MEL, melanoma; NMR, nuclear magnetic resonance; P_{eff}, effective permeability; PVDF, polyvinylidenfluoride; RAMAN, Raman spectroscopy; RAMEB, randomly methylated-β-cyclodextrin; ROS, reactive oxygen species; SEM, scanning electron microscopy; SBE, sulfobutylether-β-cyclodextrin sodium salt; SRB, Sulforhodamine B assay; WT, wild type; XRD, powder X-ray diffractometry.

* Corresponding author.
E-mail addresses: benko.beata@phd.semmelweis.hu (B.-M. Benkő), toth.gergo@semmelweis.hu (G. Tóth), moldvai.dorottya@phd.semmelweis.hu (D. Moldvai), kadar.szabina@semmelweis.hu (S. Kádár), szabo.edina@vbk.bme.hu (E. Szabó), zoltan.szabo@umfst.ro (Z.-I. Szabó), kraszni.marta@semmelweis.hu (M. Kraszni), lajos.szente@cyclolab.hu (L. Szente), bela.fiser@uni-miskolc.hu (B. Fiser), sebestyen.anna@semmelweis.hu (A. Sebestyén), zelko.romana@semmelweis.hu (R. Zelkó), sebe.istvan@semmelweis.hu (I. Sebe).

https://doi.org/10.1016/j.ijpharm.2024.124187
Received 25 March 2024; Received in revised form 22 April 2024; Accepted 29 April 2024
Available online 1 May 2024

screening experiment serves as a proof of concept of using cyclodextrin encapsulation as a platform tool for further drug delivery development in repositioning areas.

1. Introduction

Current multiparametric strategies such as computational omics-based approaches, molecular docking, network analysis, artificial intelligence, together with experimental and retrospective data analysis enable the rapid screening of drugs for their potential repositioning for unmet medical needs, such as the field of oncology (Hua et al., 2022; Wieder & Adam, 2022; Würth et al., 2016). However, drug repositioning is delayed by a few challenges, such as the identification of the new mechanism of action, bioavailability of drug in the new indication area, etc., thus most of drugs stay before phase II clinical trial, which is still far away from extensive patient care (Hua et al., 2022).

A representative candidate for anticancer repurposing is disulfiram (DIS), facing translational issues (Farooq et al., 2019; Lu et al., 2021; Lu et al., 2022; Zhao et al., 2021). A wide range of preclinical studies has demonstrated broad anticancer activity across different tumor types, and there have been several clinical trials for investigating DIS treatment efficacy (Halatsch et al., 2021; Huang et al., 2016; Huang et al., 2018; Huang et al., 2019; Kelley et al., 2021; Mego et al., 2022; Nechushtan et al., 2015; Schweizer et al., 2013; Werlenius et al., 2023), however, a breakthrough is still awaited. The reposition of DIS as an anticancer agent is limited by tumor-dependent factors, e.g., biological barriers (e.g., tumor localization and environment, resistance mechanisms, etc.), and by drug-dependent factors, such as the poor oral bioavailability and rapid unwanted metabolism (Benkő et al., 2023; Lu et al., 2022; Ramadhani et al., 2014). Presenting low aqueous solubility (4 mg/l) and high lipophilicity (logP = 3.88), accompanied by elevated membrane permeability, DIS is classified as a Biopharmaceutical Classification System (BCS) class II drug, which means that bioavailability is solubility dependent (Qu et al., 2021; Ramadhani et al., 2014). The known pharmacology in alcohol dependence is unrepresentative for oncological use, the metabolic mechanism of oral DIS in the liver explains the success in alcohol dependence, but fails to achieve the same efficacy in tumor targeting (Lu et al., 2022). To bridge the gap between *in vitro* bioactivity and *in vivo* efficacy, an essential issue to be addressed is drug delivery (Benkő et al., 2023; Lu et al., 2022; Zhao et al., 2021).

Cyclodextrins (CD) are enzyme-modified starch derivatives capable of forming non-covalent host (H) – guest (G) type of inclusion complexes with suitable lipophilic substances, improving the solubility, bioavailability, and stability of hydrophobic drugs (Brewster & Loftsson, 2007; Dhiman & Bhatia, 2020; Szente & Fenyvesi, 2017). The encapsulation process favors the dissolution in the aqueous phase, protects the drug from chemical and enzymatic degradation, limits the toxic effects, and in certain cases, act as penetration enhancers, by interacting with membrane components and inducing a perturbation in the lipid bilayer affecting the membrane properties such as fluidity and permeability (Brewster & Loftsson, 2007; Dhiman & Bhatia, 2020; Szente & Fenyvesi, 2017).

For drug repositioning strategies, the pharmaceutically relevant CDs and their inclusion complexes with the already approved chemical entities are advantageous, optimizing the innovation triangle — basic research, applied research and drug development. The status of DIS anticancer repositioning leads to the hypotheses that, as a promising tool, by CD encapsulation the solubility of the BCSII drug is significantly increasable, the prepared inclusion complexes ensure favorable bioavailability and sufficient proliferation inhibitory activity of the drug. Therefore, the present study aims to evaluate the inclusion complexation of DIS with various CDs from preparative, analytical and *in vitro* biological perspectives, determining the dose–effect curve on glioblastoma (GB) and melanoma (MEL) cell lines, emphasizing the role of molecular encapsulation of DIS with CDs in its repositioning strategy as a potential anticancer drug.

2. Methods

2.1. Materials

DIS (Mw = 296.54 g/mol, purity 97 %) was obtained from Sigma-Aldrich Chemie GmbH (Schnelldorf, Germany). All native CDs (α-, β- and γ-CD with Mw = 972.9, Mw = 1135, Mw = 1297.2 g/mol, respectively) and their derivatives: hydroxypropyl-β-cyclodextrin (HPBCD) with different degrees of substitution (DS) ~ 3, 4.5, 6 (with Mw = 1309.3, Mw = 1387, Mw = 1483.6 g/mol, respectively); randomly methylated-β-cyclodextrin (RAMEB) DS ~ 12 (Mw = 1303 g/mol), sulfobutylether-β-cyclodextrin sodium salt (SBE) DS ~ 6.5 (Mw = 2163.3 g/mol) were the products of Cyclolab R&D Ltd. (Budapest, Hungary). Ethanol (EtOH) was purchased from Molar Chemicals Ltd (Halásztelek, Hungary), methanol (MeOH), deuterated methanol (CD_3OD), deuterium oxide (D_2O), acetonitrile (ACN) and dimethyl sulfoxide (DMSO) were ordered from Sigma-Aldrich Hungary (Budapest, Hungary). Ultrapure, deionized water was prepared by a Milli-Q Direct 8 Millipore system (Milford, MA, USA), Aqua ad iniectabilia, gentamycin 80 mg/2 ml injection (Sandoz GmbH, Kundl, Austria), and 2 ml syringes were from University Pharmacy Department of Pharmacy Administration, Semmelweis University. Glioblastoma cell line (U251MG, ECACC-09063001) was a kindly provided by William P J Leenders (Department of Biochemistry, Radboud University Medical Center, Nijmegen, The Netherlands) in a collaborative work (Hujber et al., 2018). Melanoma cell line (A2058, ECACC-91100402) was a gift from Chemotaxis Research Group, Semmelweis University, led by László Kőhidai. For the cell cultures, Dulbecco's Modified Eagle Medium (DMEM) High Glucose (HG) with Sodium Pyruvate basal media, supplemented with 10 % foetal bovine serum (FBS), 2 mM L-glutamine, and 100UI/ml penicillin–streptomycin, was obtained from Biosera (Nuaille, France). Acceptor Sink Buffer and microFlux polyvinylidenfluoride (PVDF) hydrophobic membranes were purchased from Pion Inc. Ltd. (East Sussex, UK). Hydrophilic PTFE syringe filters, with 13 mm and 25 mm diameter and 0.45 μm pore size were ordered from Lab-Ex Ltd. (Budapest, Hungary). All other chemicals used were of analytical grade from commercial suppliers.

2.2. Cyclodextrin screening, phase solubility analysis and complex stability determination

The first step is to investigate whether there is an interaction between the selected drug and the different CD types, thus for the CD-screening, native (α-, β-, γ-CD) and β-CD derivatives (HPBCD with DS 3, 4.5 and 6, RAMEB DS ~ 12 and SBE DS ~ 6.5) were selected. To measure whether the solubility of the G molecule, which is otherwise poorly soluble in water, increases in the presence of the H molecule, phase-solubility analysis was performed according to the method described by Higuchi and Connors (Higuchi & Connors, 1965). An excess amount of DIS (80 mg) was added to 5 mL water (without any buffer) containing increasing concentrations of CDs (0, 3, 6, 15, 18, 24, 27, 30 mM for each CDs, except β-CD, where 0, 2, 3, 4, 6, 8, 9 12 mM were used, due to its limited solubility in water). The obtained suspensions were stirred for 24 h at 25 °C. DIS concentrations were measured from the filtered suspensions (13 mm PTFE 0.45 μm syringe filter) with a HPLC, based on USP DIS assay method (Supporting Information).

2.3. Liquid state characterization

2.3.1. Capillary zone electrophoresis (CZE)

For the confirmation of the obtained equilibrium constant (K_{stab}) value from phase solubility analysis, a capillary electrophoresis method was applied in case of inclusion complexation with SBE. The experiment was performed with Agilent 7100 capillary electrophoresis instrument equipped with ChemStation software. The untreated fused-silica capillary (Agilent, Waldbronn, Germany) with 363 μm outer and 50 μm inner diameter, and 48.5 cm total and 40 cm effective length was conditioned at the beginning by flushing with 1 M NaOH for 30 min followed by 0.1 M NaOH and water for 20 min each. Prior to all runs the capillary was preconditioned by flushing with 0.1 M NaOH (2 min), water (1 min), and background electrolyte (BGE) (2 min). The experiments were performed with increasing concentrations of the complexing agent in the BGE, while the constant concentration of analyte was injected as a sample (Beneš et al., 2012). The electrophoretic conditions were as follows: voltage + 20 kV, capillary temperature 25 °C, UV detection with photodiode array detector at 210, 230, and 250 nm, hydrodynamic injection (50 mbar for 3 s) at the anodic end of the capillary (Supporting Information).

2.3.2. Determination of complex stoichiometry using UV-Job plot method

The complex stoichiometry of DIS with β-CD, RAMEB and SBE was carried out with UV/VIS spectroscopy, using a Jasco V-550 UV/VIS spectrophotometer with 10-mm quartz cuvettes at 25 °C, using the solvent system ACN:H_2O 1:20. Equimolar solutions of DIS and CDs were mixed to standard volume and proportions such that the total concentration remained constant, and the G/H molar ratio was varied from 0 to 1. The absorbances at 250 nm for each molar ratio were measured (Supporting Information).

2.3.3. Determination of complex stoichiometry using nuclear magnetic resonance (NMR) investigations

Using 1H NMR measurements, an additional Job plot was investigated for the determination of DIS and β-CD complex stoichiometry. Spectra were recorded at 20 °C on a Varian (Varian, Palo Alto, California, US) Mercury Plus spectrometer (400.0 MHz for 1H) equipped with a broadband (Varian ATP) probe-head with z-gradient, using the solvent system CD_3OD:D_2O 3:2. Each spectrum was collected in 16,384 data points using 32–128 scans with a spectral window of 2801 Hz and referenced to the methanol signal. The two-dimensional phase-sensitive rotating-frame Overhauser effect spectroscopy (2D ROESY) NMR technique was applied to gain structural information about the inclusion complex, studying the interactions between the protons of the DIS and the CD cavity protons with Bruker Avance III HD 600 NMR spectrometer (Bruker, Billerica, Massachusetts, US) equipped with a 5 mm BBO probe head with z-gradient and TopSpin3.5pl7 software. The 2D ROESY spectrum of the 1:5 DIS:β-CD complex was recorded at 25 °C. The Bruker roesyphpr.2 pulse sequence was used with a mixing time of 300 ms and a spectral width of 7 ppm in both dimensions. The spectrum was acquired into 1024 complex points in t2 with 112 scans coadded at each of 206 t1 increments. The spectrum was processed to 2048 × 1024 data points (Supporting Information).

2.4. Preparation of inclusion complexes and solid-state characterization

2.4.1. Preparation of inclusion complexes and the respective physical mixtures

Based on phase solubility study results, inclusion complexes of DIS were prepared with HPBCD, RAMEB and SBE in 1:2.5 (DIS:CD) mole ratio with co-dissolution (DIS + HPBCD, DIS + RAMEB) or hetero-phasic (DIS + SBE) methods according to the component s solubility properties in EtOH (HPBCD, RAMEB) and water (SBE). To achieve an adequate yield of manufacturing and stability of product, a higher mole ratio was used than the complex stoichiometry (Supporting Information). In case of HPBCD and RAMEB the co-dissolution method was used. CDs and DIS were separately dissolved in EtOH, then solutions were mixed under continuous stirring for 24 h at 25 °C. The solvent was removed by evaporation, using rotary evaporator (BÜCH Rotavapor R-200, Switzerland) on 40 °C, 20–25 min. The product was redissolved in water, filtered (25 mm PTFE 0.45 μm syringe filter), frozen and lyophilized with Scanvac CoolSafe (Labogene, Denmark) freeze dryer at −55 °C, for 24 h. In case of SBE, due to its limited solubility in EtOH, hetero-phasic method was applied. SBE was dissolved in water, and DIS powder was added to the CD-aqueous solution and stirred for 24 h at 25 °C, then filtered, frozen and lyophilized under the same conditions. The obtained powders were gently ground with mortar and pestle and were kept in a vacuum desiccator (Duran Vakuumfest desiccator plate, Value vacuum pump, V-i240Y-R32 model) at room temperature until use. For comparative analysis, the physical mixtures were prepared in the same molar ratio in a ceramic mortar.

2.4.2. Differential scanning calorimetry (DSC)

DSC method was applied to examine the crystalline/amorphous character of the initial components and the inclusion complex products. The samples were measured into a 40 μL pierced aluminum pan with weight of 10 ± 0.5 mg, then a traditional linear heating DSC method (DSC3 + device, Mettler Toledo AG, Zürich, Switzerland) was applied from 25 °C to 200 °C with a heating rate of 10 °C/min. The DSC chamber was purged with dry nitrogen using a flow rate of 50 ml/min (Supporting Information).

2.4.3. Powder X-ray diffraction study (XRD)

The X-ray diffraction spectra of DIS, HPBCD, RAMEB, SBE, prepared inclusion complexes, and the respective physical mixtures were analyzed with PANalytical X'Pert3 Powder diffractometer, PANalytical Data Collector Application, and HighScore program (Malvern Panalytical Ltd., UK). Cu Kα radiation with 45 kV accelerating voltage and 40 mA anode current over the range of 2–80°[2θ] was used, applying 0.0080°[2θ] step size and 100 s times per step in reflection mode, spinning the sample holder by 1 s^{-1}. Incident beam optics were as follows: programmable divergence slit with 15 mm constant irradiated length; anti-scatter slit at fixed 2°[2θ].

2.4.4. Scanning electron microscopy (SEM) images

A JEOL JSM 6380LA type scanning electron microscope (JEOL, Tokyo, Japan) was applied to investigate the morphology of DIS, CDs, inclusion complexes, and the respective physical mixtures. A conductive double-sided carbon adhesive tape was used for fixing the samples to the sample holders and for avoidance of electrostatic charging, a thin layer of conducting gold was sputtered to the surface of the samples with a JEOL 1200-type equipment (JEOL, Tokyo, Japan). The SEM measurements were conducted as follows: accelerating voltage was adjusted to 10 kV, the applied working distance was 16–17 mm, and the spot size was 40 nm.

2.4.5. Attenuated total reflectance Fourier-Transform infrared spectroscopy (ATR-FTIR)

The ATR-FTIR spectra were determined by a Jasco FT/IR-4600A instrument with ATR Pro ONE accessory (JASCO Ltd., Tokyo, Japan) over the range of 400 – 4000 cm^{-1} at a resolution of 4 cm^{-1}. Deuterated triglycine sulfate (DTGS) detector was used and 64 scans were accumulated for each composition. Background spectra were recorded and subtracted from the samples.

2.4.6. Raman spectroscopy (RAMAN)

RAMAN spectra were collected using a Perkin Elmer 2000 NIR FT − Raman system (PerkinElmer Inc., Waltham, MA, USA) equipped with a diode pumped Nd:YAG laser PSU and Spectrum v5.0.1 software. Each spectrum was collected in the spectral range of 3500 to 100 cm^{-1}, applying 32 scans with 1 cm^{-1} interval, 4 cm^{-1} resolution wand a laser

power 925mW for CDs and 500mW for pure drug, physical mixtures and inclusion complexes (Supporting Information).

2.5. In vitro biological characterization

2.5.1. Small volume dissolution and permeation analysis

2.5.1.1. Dissolution. Comparative *in vitro* dissolution studies were performed from the lyophilized inclusion complexes, physical mixtures and raw active (DIS) with Rainbow Dynamic Dissolution Monitor μDISS Profiler (Pion Inc Billerica MA, USA), equipped with 6 fiber optic UV probes, enabling real-time monitoring of the analyte's *in situ* concentration. Powder samples, were weighed direct in sample vessels and were set to instrument, inserting fiber optic UV dip probes and adding 10 mL of PBS (20 mL PBS supplemented with 20 % HPBCD in case of pure DIS) under continuous stirring with a magnetic stirrer. From each sample, 3 parallel measurements were performed. Previously determined calibration data and second derivative spectra were used to evaluate DIS s concentration (Supporting Information).

2.5.1.2. Dissolution-permeation. The permeability of lyophilized inclusion complexes, the respective physical mixtures, and raw DIS were tested using μFLUX (Pion Inc., Billerica MA, USA) apparatus, consists of a donor and an acceptor chamber separated by an artificial membrane (PVDF, 0.45 μm, 1.54 cm^2) impregnated with 25 μL n-dodecane to form a lipophilic barrier between the donor and acceptor chambers. The acceptor chamber, representing the blood circulation, was filled with 20 ml Acceptor Sink Buffer (ASB, Pion Inc., Billerica MA, USA). For the donor chamber, adapting the method described by Bartos et al. (Bartos et al., 2021), 20 ml of pH 5.6 PBS was prepared. Samples equivalent to 75 μg/ml of DIS were placed in the donor chamber, and both chambers were stirred with a magnetic stirrer (speed 250 rpm) at 37 °C. To evaluate the concentration of DIS calibration was conducted using the same tip types adjusted to the fiber optic UV dip probe employed in previous experiment (Supporting Information).

2.5.2. In vitro proliferation Assays— Alamar Blue (AB) and Sulforhodamine b (SRB) assays

Cells were cultured using DMEM high glucose basal media for both cell lines (U251MG wt, A2058 wt), supplemented with 10 % FBS, 2 mM L-glutamine and antibiotics. For the proliferation assays, cells were seeded 24 h prior to treatment onto 96-well plates (2500 cells/100 μl for U251MG wt and 3000 cells/100 μl for A2058). The 72 h treatment course consists of addition of sample solution from DIS:HPBCD and DIS:RAMEB and DIS:SBE inclusion complexes in a dose range of the drug between 0.01 nM − 100 μM for U251MG wt and 0.01 nM − 1 μM for A2058, also using blank, control and control + CD samples. To monitor the effect of the treatments on cell growth and cellular metabolic activity, the AB and SRB assay were applied, adapting the respective protocols from Dankó et al. (Dankó et al., 2021) (Supporting Information).

2.6. Molecular modelling

Molecular modelling is a computational method to study the structural features of molecules, used in CD chemistry to elucidate the atomic details of complexation, to gain insights into the behavior of these molecules and their interactions with other substances. The β-CD derivatives, HPBCD, RAMEB, SBE, present an un-conserved structure, as the respective functional groups, –OH, $–CH_3$, sulfobutylether, are randomly arranged on the β-CD skeleton and the CD itself is a mixture of derivatives with different degrees of substitution, requiring the prediction of a great number of isomers. Thus, β-CD was selected as a model to determinate the interaction between DIS and CDs. Energy minimization of the β-CD was performed by using the OPLS-AA forcefield in combination with the Generalized Born implicit solvation model. DIS model was built and conformational search was carried out by using the OPLS-AA forcefield in combination with the Generalized Born implicit solvation model. The lowest energy conformer of DIS was selected and docked into the minimized β-CD model by applying a "blind docking" protocol (Hetényi & van der Spoel, 2002) which was carried out by using AutoDock Vina (Trott & Olson, 2010). The grid box dimensions were set to 40x40x40 Å, significantly surpassing the actual size of the host. Parameters for exhaustiveness and the maximum number of binding modes were selected to be to 8 and 9, respectively. The binding mode with the lowest energy was then chosen, and the properties of the associated structure were subsequently analyzed.

2.7. Data analysis and statistics

Data collection, analysis and visualization were performed with Office package and the non-linear regression analyses (dose–response curves) were conducted using Origin 9.5 (OriginLab Corp., Microcal Software, Inc., Northampton, MA, USA). The standard deviation values were calculated with n = 3 in each experiment. To verify, if there is any significant difference between IC_{50} values of the three types of inclusion complexes, obtained from the two proliferation assays and calculated on each passage number of cells, a two-way ANOVA, associated with Tukey test was applied in Origin (Supporting Information).

3. Results

3.1. Preparation and analytical characterization

3.1.1. Phase solubility analysis and complex stability determination

As a preliminary investigation, a CD-screening method was applied with the native CDs (α-, β-, γ-CD) to confirm DIS's accessibility in the different cavity sizes. DIS formed no complex with α-CD, nor with γ-CD, and with β-CD just a slight tendency was observed, associated with the natural CD's limited solubility, self-assembling, and aggregating properties (Saokham et al., 2018). Consequently, the more soluble β-CD derivatives, HPBCD, RAMEB and SBE were included in the isotherm analysis. In the case of HPBCD, RAMEB, and SBE linear phase solubility diagrams were observed (Fig. S2, Supporting Information). The calculated values of the K_{stab} are used to compare the affinity of the drug for different CDs, representing a fundamental property that describes the strength of an interaction between H and G molecules (Jambhekar & Breen, 2016b). However, the value of K_{stab} is highly sensitive towards small changes in intrinsic solubility (S_o) of a drug and for poorly-soluble ones such as DIS it can be complicated to obtain exact S_o values, therefore under such conditions, the determination of complexation efficiency (CE) is more accurate (Saokham et al., 2018). The highest K_{stab} and CE were achieved with RAMEB (Table 1). The observed values for K_{stab} are usually between 50 and 2000 M^{-1} (Loftsson et al., 2005); the inclusion complexes of DIS with β-CD derivatives are included close to the upper limit of this interval. In the case of SBE, an additional K_{stab} determination was conducted with CZE, achieving a 10-fold higher K_{stab} value ($\log K_{stab} = 4.4$), explicable with a deviation of the So value, but calculated with water solubility of DIS known from literature (0.0135 mM) the values were convergent ($\log K_{stab} = 4.8$). In the case of HPBCD the different DS type compounds gave different K_{stab} values with DIS. The highest value was found with the DS ~ 4.5, the DS 3 and 6 lead to a decrease in K_{stab}, explicable with the unique configuration of CDs, which imparts in creating the thermodynamic driving force required to form a H-G complex (Jambhekar & Breen, 2016a). Szabó et al. observed a similar phenomenon when studying pomalidomide CD complexation (Szabó et al., 2021). The solubility of the BCS II drug by encapsulation with β-CD derivatives was significantly increased (~1000 folds). Based on the presented results the CE order of β-CD derivatives is as follows: RAMEB > SBE > HPBCD DS ~ 4.5 > HPBCD DS ~ 3 > HPBCD DS ~ 6 (Table 1).

Table 1
The isotherm type, calculated complexation efficiency, equilibrium constants, and the achieved solubility enhancement based on phase solubility study.

CD type	DS	Type of phase-solubility diagram	Equation	Standard error	CE	K_{stab} [M^{-1}]	Maximum solubility enhancement [maximum applied CD concentration]*
α-CD	–	X	–	–	–	–	–
β-CD	–	B_S	–	–	–	–	106 (12 mM)
γ-CD	–	X	–	–	–	–	–
HPBCD	3	A_L	y = 0.3372x + 1.0869	Intercept:0.50 Slope:0.03	0.5	468	900 (30 mM)
	4.5	A_L	y = 0.3379x + 1.0026	Intercept:0.56 Slope:0.03	0.5	509	916 (30 mM)
	6	A_L	y = 0.2809x + 0.7947	Intercept:0.43 Slope:0.02	0.4	492	752 (30 mM)
RAMEB	12	A_L	y = 0.6116x + 0.7621	Intercept:0.41 Slope:0.02	1.6	2066	1473 (30 mM)
SBE	6.5	A_L	y = 0.5006x + 0.6122	Intercept:0.35 Slope:0.02	1.0	1637	1213 (30 mM)

Notes: Types of phase-solubility diagrams are classified according to Higuchi and Connors (Higuchi & Connors, 1965): AL = linear diagram, BS = complex with limited solubility, X = no complexation. *The maximum solubility enhancement is calculated at maximum applied CD concentration with DIS water solubility, known from literature: 0.0135 mM.

3.1.2. *Complex stoichiometry determination and molecular modelling*

In general, when the slope of the linear diagram (A_L-type plot) is less than unity, a 1:1 complex is formed. Conversely, if the slope is greater than unity, higher-order complexes are assumed to be involved in the solubilization process (Jambhekar & Breen, 2016a). Although a slope of less than unity does not exclude the possibility of higher order complexes (Jambhekar & Breen, 2016a), therefore to study the complex stoichiometry supplementary investigations also should be applied to demonstrate the 1:1 complex formation. Analyzing the structure of DIS, the molecular size of the drug excluded the chance of complex formation with more than one CD molecule, however, the symmetry of DIS raises several issues about the inclusion process. The structural information makes the prediction of stoichiometry quite straightforward and accurate, thus, in modern supramolecular chemistry it is advantageous to use 2D-NMR and molecular modelling to obtain detailed information about the structure of the host, guest and host–guest complex itself (Thordarson, 2011). The spatial arrangement was deciphered with 2D ROESY studies, investigating spatial proximity between nuclei of DIS and β-CD, by observing intermolecular dipolar interactions. A cross-peak between the $-CH_3$ signals of DIS and the H3 signal of β-CD was observed (Fig. 1a green frame), suggesting a deep insertion of DIS in the cavity of β-CD, presumably from the wider rim. The complexation of DIS with β-CD was further studied by molecular modelling, spotting the accordance between the theoretical calculations and the experimental results. Docking simulations confirmed the proposed spatial structure of the inclusion complex, the half part of the symmetrical molecule ($-CH_3$ indicates one end of the drug) is incorporated in the β-CD cavity. The calculated binding energy (EA) is negative (−3.5 kcal/mol) which indicates favorable complexation via mainly dispersion interaction between DIS and the skeleton of β-CD (Fig. 2). The Job plot method is a fast, easy, and reliable technique for determining complex stoichiometry, widely employed in the determination of cyclodextrin complex stoichiometry (Jullian et al., 2008; Sid et al., 2021; Sravani et al.; Tóth et al., 2017). The widely used supramolecular titration, Job's continuous variation

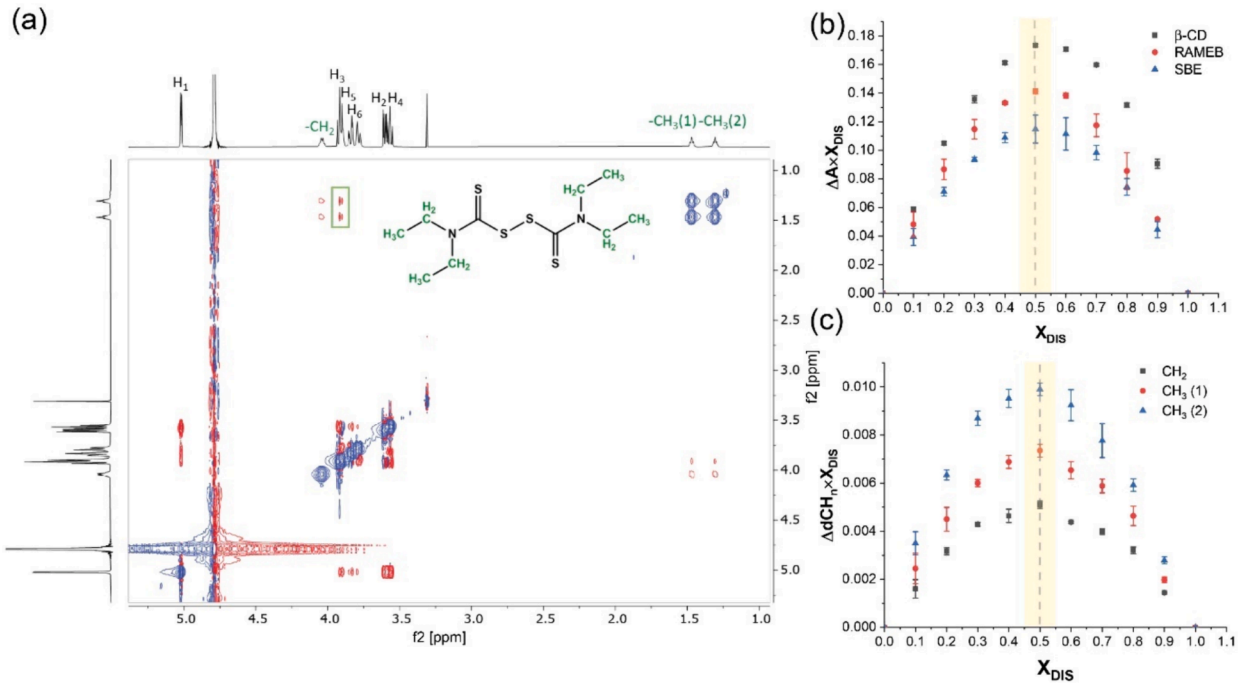

Fig. 1. Stoichiometry determination with 2D-ROESY (a), and UV- (b) and NMR- (c) Job plot methods of DIS and β-CDs. On 2D ROESY spectrum of DIS and β-CD the assignments for β-CD are in black, for DIS are in green. The intermolecular ROESY cross-peaks between C3-H of β-CD and the methyl signals of DIS are in green rectangle.

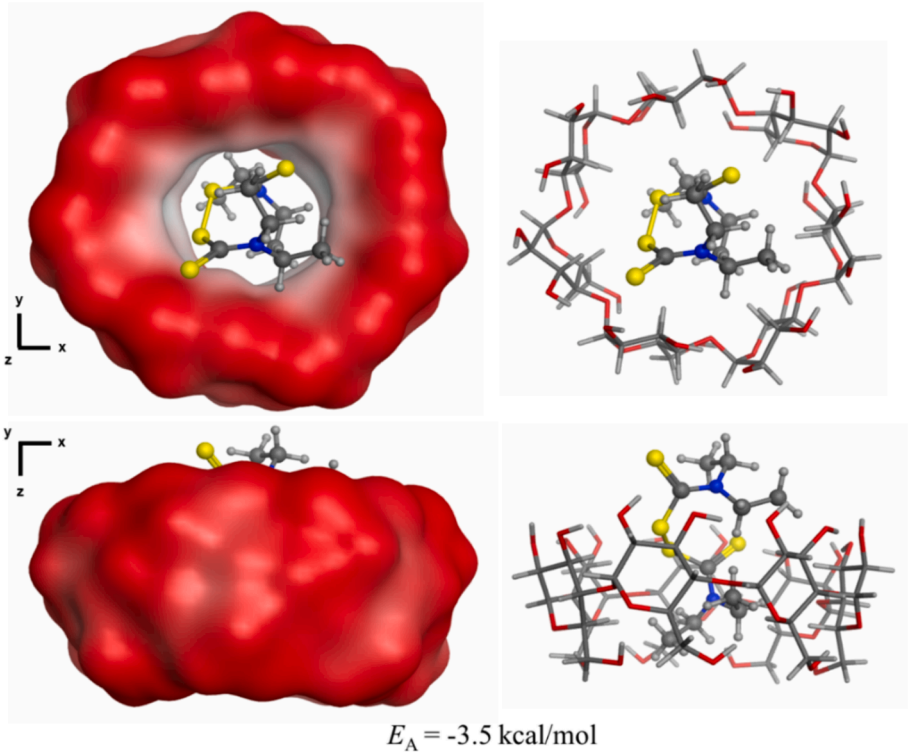

Fig. 2. Molecular modelling of spatial conformation of the DIS and β-CD inclusion complex and corresponding binding energy.

method, was complementary employed to confirm the findings obtained from NMR (2D-ROESY), phase-solubility measurement, and molecular docking studies. The stoichiometry of the inclusion complexes of DIS with β-CD using NMR spectroscopy, and with β-CD, RAMEB, and SBE, using UV spectroscopy was evaluated. To obtain the Job plot diagrams the absorbance or chemical shift changes in the presence and absence of CDs were followed and the calculated factors from this (ΔA^*X_{DIS}, $\Delta\delta^*X_{DIS}$) were plotted as a function of DIS molar ratio (X_{DIS}). With both methods and with all the applied CDs the curves reached the maximum at 0.5, indicating 1:1 binding stoichiometry (Fig. 1b and c). Job plot method has some known limitations (Ulatowski et al., 2016), e.g., the determination of association constants and stoichiometry from supramolecular titration really only works well when there is one type of complex present (usually the 1:1), when there is more than one complex, the Job's method becomes unreliable and also fails when either the H or G aggregates in solution (Thordarson, 2011). However, supplementing it with other techniques yields appropriate results. All the applied approaches (phase solubility study, NMR analysis, molecular modelling and Job plot method) suggested a 1:1 complex formation, and these findings correlate with the results obtained by Tyukova et al. with preparative chromatography and refractometric detection (Tyukova et al., 2016).

3.1.3. Preparation of inclusion complexes and solid-state analysis

3.1.3.1. Preparation of inclusion complexes. Although, the molecular ratio of DIS and CDs is 1:1, for the preparation of a soluble product with a corresponding yield, 1:2.5 ratio was applied, in accordance with the minimum CE = 0.4, calculated for HPBCD DS ~ 6, suggesting that from 100 molecules of CDs only 40 forms complex, thus 2.5-fold more is required to achieve 100. The solid complexes were prepared by lyophilization and analyzed by complementary solid-state techniques, in comparison with the raw materials and respective physical mixtures to confirm the incorporation of DIS into the CDs cavity.

3.1.3.2. DSC. On comparative DSC thermograms of the free drug, raw CDs, lyophilized complexes, and physical mixtures (Fig. 3a), DIS was characterized by a narrow endotherm with a minimum at ~ 73 °C, corresponding to the melting point and indicating its crystalline state. The starting CDs showed no sharp endothermic peaks, due to their amorphous structure, and only a broad endotherm between 50–140 °C was observed, related to the evaporation of the absorbed water. In the case of physical mixtures, the endotherm peaks with the minimum corresponding to the melting point of the crystals of DIS appeared. The lyophilized formulations presented similar profiles to that of raw CDs, the melting peak of crystalline DIS was missing, demonstrating the amorphization of the compound and assuming the presence of molecular interaction between DIS and CDs. Similar results were previously reported in case of DIS and HPBCD and SBE (Pereira et al., 2022; Qu et al., 2021; Tyukova et al., 2020).

3.1.3.3. XRD. The XRD analysis of the pure drug displays a pattern with distinct series of accentuated peaks, indicating a crystalline structure, while HPBCD, RAMEB and SBE presented an amorphous pattern by a diffuse halo. The physical mixture contained a superimposition of strong peaks on a diffuse halo, representing the combination of crystalline (DIS) and amorphous (CDs) phases. Conversely, the patterns of the lyophilized products were lacking the crystallinity-related intense peaks and showed a pattern similar to the raw CDs, providing the conversion of the crystalline compound to amorphous, which could be the consequence of molecular encapsulation (Fig. 3b).

3.1.3.4. SEM. The SEM images of the free drug, raw CDs (HPBCD, RAMEB, SBE), and freeze-dried formulations showed different morphologies (Fig. 3c). The roughly spherical particles of DIS and the shape of different CDs cannot visible in the SEM images of the freeze-dried samples. The homogenous plate-like structure of the lyophilized formulations suggesting the new form of the inclusion complexes.

3.1.3.5. ATR-FTIR. As a further method to confirm the embedment of

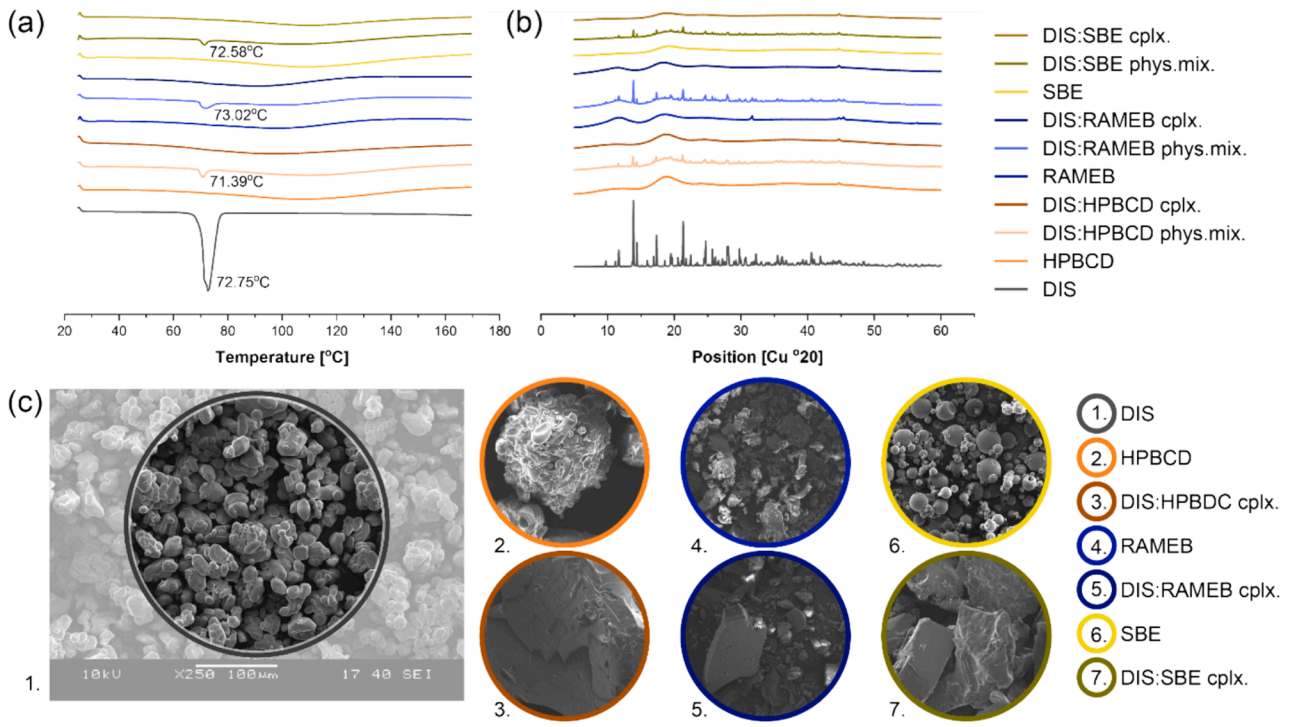

Fig. 3. The DSC (a), XRD (b) and SEM (10 kV, 250x, 100 μm) (c) analysis of the solid-state starting components (DIS, HPBCD, RAMEB, SBE), their inclusion complex and the respective physical mixtures. On DSC (a), the endotherm peaks appeared with the minimum at 71.39 °C (DIS:HPBCD physical mixture), 73.02 °C (DIS: RAMEB physical mixture), and 72.58 °C (DIS:SBE physical mixture), corresponding to the melting point of the crystals of DIS (72.75 °C). Abbreviations: cplx. = inclusion complex of DIS with respective CD, phys.mix. = physical mixture.

DIS in HPBCD's, RAMEB's or SBE's cavity, the ATR-FTIR spectra were also analyzed, comparing the presence of characteristic absorption peaks of pure DIS and raw CDs with the peak shifts of inclusion complexes and physical mixtures (Fig. 4a). The spectrum of DIS presents a characteristic peak group between 2750–3250 cm^{-1} corresponding to C–H stretching vibration, and between 1250–1500 cm^{-1} representing the CH_2 and CH_3 deformations and N-C = S and C = S bond stretching (Pereira et al., 2022; Said Suliman et al., 2021; Zhang et al., 2018). The HPBCD, RAMEB and SBE bands changed only slightly as a consequence of formation of the inclusion complex, the characteristic bands representing DIS were not significantly detected on the spectra of complexes, nor on spectra of physical mixtures, thus no difference was seen to confirm the inclusion. This may be explicable with lower content of the drug than the limit of detection of the ATR-FTIR kit, observed also by Suliman et al. and Pereira et al (Pereira et al., 2022; Said Suliman et al., 2021). Another reason could be the applied 1:2.5 (DIS:CD) molar ratio, used for the preparation of lyophilized complexes and physical mixtures, as the bands of CDs, used in higher proportion, may superposed the characteristic peaks of DIS. Only in case of samples with HPBCD a few bands were detectable, e.g., the shape of peak at 3012 cm^{-1} is intense in case of DIS and physical mixture, whereas is broader and less intense in the spectrum of the complex, suggesting that the inclusion complex was successfully prepared (Fig. 4a). Qu et al., Tyukova et al., and Pereira et al. have also reported similar results for the inclusion complexes of DIS with HPBCD and SBE (Pereira et al., 2022; Qu et al., 2021; Tyukova et al., 2020; Tyukova et al., 2016).

3.1.3.6. RAMAN. Due to the limited applicability of ATR-FTIR for the comparison of the known complexes of DIS with RAMEB and for the confirmation of the drug insertion in the rim of CDs, a RAMAN analysis was also performed. DIS presents two diethyldithiocarbamate (DEDTC) group linked with a disulfide bond, exhibiting C2-symmetry and RAMAN spectrum (Kang et al., 2002) with characteristic peaks at 437 cm^{-1}, attributed to $–CH_2NC$ deformation and C = S stretching, 558 cm^{-1} corresponding to S-S stretching, peaks between 1455–1510 cm^{-1} assigned to CH_3 deformation and C-N stretching (Kang et al., 2002; Pu et al., 2021) and 2938 cm^{-1} due to C–H stretching. Accordingly, the strongest bands at 437, 558 and 2938 cm^{-1}, were selected for the comparative analysis of the three types of samples with different CDs. The results showed a spectrum with sharp peaks in the case of pure DIS, less intense and broad peaks in the case of physical mixtures, and "disappearance" of the characteristic peaks of the drug and a similar spectrum to the respective β-CD derivative in the case of complexes. These findings suggest the inclusion of the G molecule in the cavity of the H, and the formation of amorphous structure, correlating with the XRD and DSC results. The RAMAN spectroscopy surpasses the sensitivity of FTIR for the analysis of inclusion complexes formed with DIS and various CDs (Fig. 4b).

3.2. *In vitro biological characterization*

3.2.1. *Small volume dissolution and permeation analysis*

Comparative studies were conducted to assess dissolution improvement, with the lyophilized samples, respective physical mixtures, and the pure crystalline DIS. The obtained curves show a remarkable difference between the samples, the dissolution from the lyophilized powder was rapid, it reached its maximum in about 1 min. While the dissolution from the physical mixtures was improved compared to the pure drug, 60 min was not enough time to reach the equilibrium concentration. In stark contrast, the raw crystalline DIS presented the lowest dissolution tendency. The dissolution behavior of the freeze-dried formulations with the three different types of β-CD derivatives varied slightly, the complex with RAMEB liberated the highest DIS quantity, followed by SBE and HPBCD (Fig. 5a). The observed dissolution profiles converge with CE values of the complexes, the higher CE assuring a higher concentration of DIS. The deviation from the pre-set theoretical value of the lyophilized samples is derived most probably from the preparation procedure yield, while in the case of the physical mixtures,

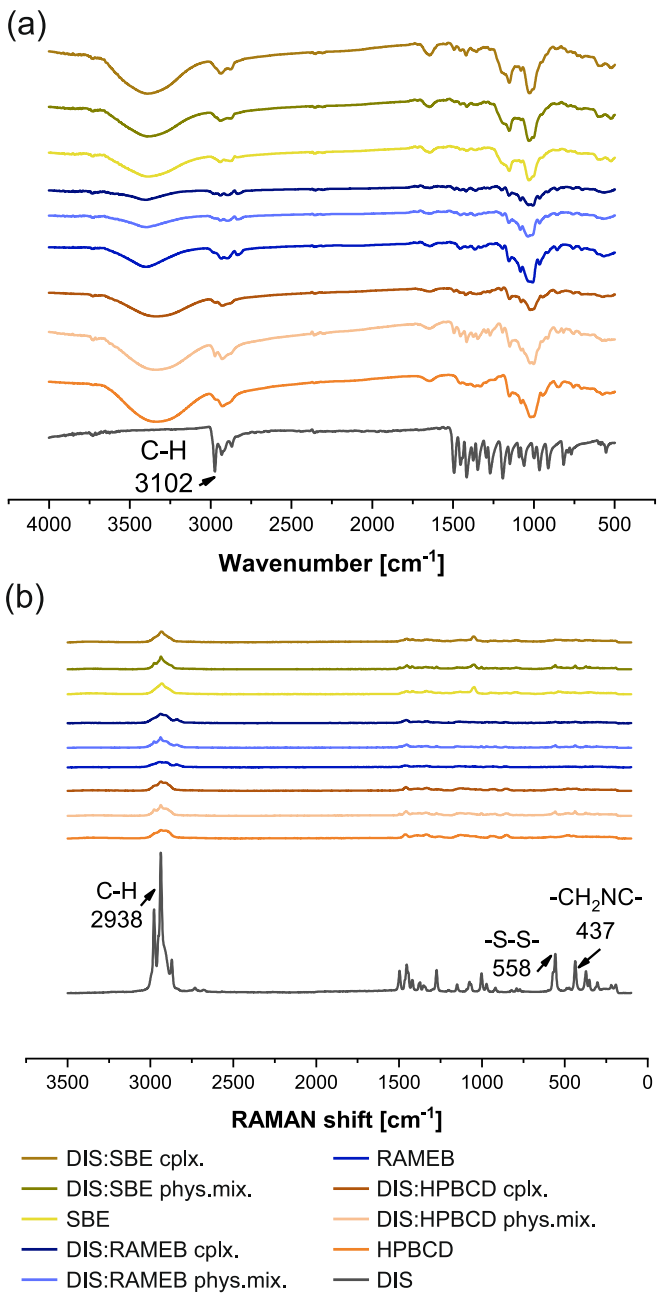

Fig. 4. The FTIR (a) and RAMAN (b) spectra of DIS, HPBCD, RAMEB, SBE, their inclusion complexes and the respective physical mixtures. Abbreviations: cplx. = inclusion complex of DIS with respective CD, phys.mix. = physical mixture.

it is probably given by the time-dependent complexation equilibrium.

The permeability behavior of the inclusion complexes was the exact reversed case of dissolution: the HPBCD complex presented the highest, whereas RAMEB the lowest permeability profile. In all the cases the physical mixtures lagged from the inclusion complexes and as expected, the lipophilic pure drug presented an extremely elevated permeability through the artificial membrane (Fig. 5 b, c). The permeability order of inclusion complexes is related to the values of their K_{stab}, showing a reverse proportion, i.e., the lower the K_{stab}, the higher the effective permeability (P_{eff}). The K_{stab} describes the affinity of drugs for different CDs, e.g., the strength of an interaction between a G and a H (Jambhekar & Breen, 2016b). While a complex is being formed, no covalent bonds are formed or broken, and drug molecules in the complex are in rapid equilibrium with free molecules in the solution (Jambhekar & Breen, 2016a, 2016b). The initial equilibrium to form a complex is rapid, however, the final equilibrium takes a longer time to attain, as the drug molecules, once inside the CD cavity, undergo conformational adjustments to take maximum advantage of the presence of weak Van der Waals forces (Jambhekar & Breen, 2016a). Thus, if the K_{stab} presents a low value, the complex formation is decreased, while the proportion of the free drug in this equilibrium system is increased and according to its *logP* traverses the lipid barrier, therefore the HPBCD complex of DIS presents more favorable permeability behavior than RAMEB (Fig. 5c). The P_{eff} value is derived from the flux [$J(t)$] across the membrane and from donor-side concentration, however on acceptor side of the artificial membrane, the concentration of DIS was significantly higher in case of lyophilized samples than the physical mixtures or the crystalline material (Fig. 5d). This difference between the formulated and non-formulated drug could be noticed from their flux-profile, as in the evaluated time period, the $J(t)$ of the pure drug was under 0.5, whereas the CD inclusion complexes above 1, suggesting that more than 2 times more molecules went through the membrane from the CD formulations than from the original crystalline DIS (Fig. 5d). During the evaluated time frame, the permeability profile of the physical mixtures not only trailed behind but fully tracked down the profile of respective CD formulations, while the flux-profile also lagged, but the order of physical mixtures differs from the inclusion complexes, explicable with the mentioned time-dependent K_{stab} evolution (Jambhekar & Breen, 2016a).

3.2.2. *In vitro proliferation Assays—AB and SRB assays*

The cell line selection was based on an overview of the clinical trials with DIS in cancer indication (Supporting Information, Table S10). Based on ClinicalTrials.gov database from 2023 October, the clinically most researched target tumor types are GB and MEL (Fig. 6a); and the conducted clinical trials are almost 50 % completed (Fig. 6b). The present research compares the proliferation inhibitory activity of the synthesized inclusion complexes of DIS with the three pharmaceutically important CDs (HPBCD, RAMEB, SBE) on selected cell lines, U251MG wild type (wt) and A2058, representing the two clinically most interested areas. For GB, U251MG was preferred representing isocitrate dehydrogenase wild-type (wt) properties correlating with therapy resistance (Alifieris & Trafalis, 2015; Cheng et al., 2013; Ichimura et al., 2009). For MEL, A2058 was chosen, which was isolated from a lymph node metastasis, representing the hard-to-treat phase of cancer, highlighting that MEL has a high propensity to metastasize to the brain (Gampa et al., 2017; Lopes et al., 2022). In all the cases, the same tendentious proliferation inhibition was observed using either the AB assay or SRB test. However, a conspicuous difference in treatment response rate could be observed between the two cell lines, as IC_{50} values in the case of U251MG wt were approximately around 7000 nM, while in the case of A2058, a concentration around of 100 nM already reduced cell viability with 50 % (Table 2). Based on the proliferation results with the IC_{50} of different inclusion complexes, the sample with RAMEB stands out, as it produced a slightly higher proliferation-reducing effect than complexes with HPBCD or SBE on both cell lines, measured with both assays (Table 2). However, at the level of 0.05, there is no significant difference between the IC_{50} values of the three types of inclusion complexes on the respective cell line [U251MG wt: degrees of freedom (DF) for inclusion complexes 2, $F = 2.34$, $p = 0.13$; A2058: DF = 2, $F = 2.24$, $p = 0.14$]. Cells treated with CDs alone, used as a control, did not show significant changes, suggesting that CDs did not have an inhibitory effect on cell proliferation (Fig. 6 c, d), which, together with IC_{50} value comparisons, suggest that the effect can be attributed only to the pharmacodynamic properties of drug, without Cu^{2+} supplementation.

4. Discussion

4.1. *Anticancer repositioning of DIS*

The discovery of DIS as a drug has been dated as the late 1940s, first

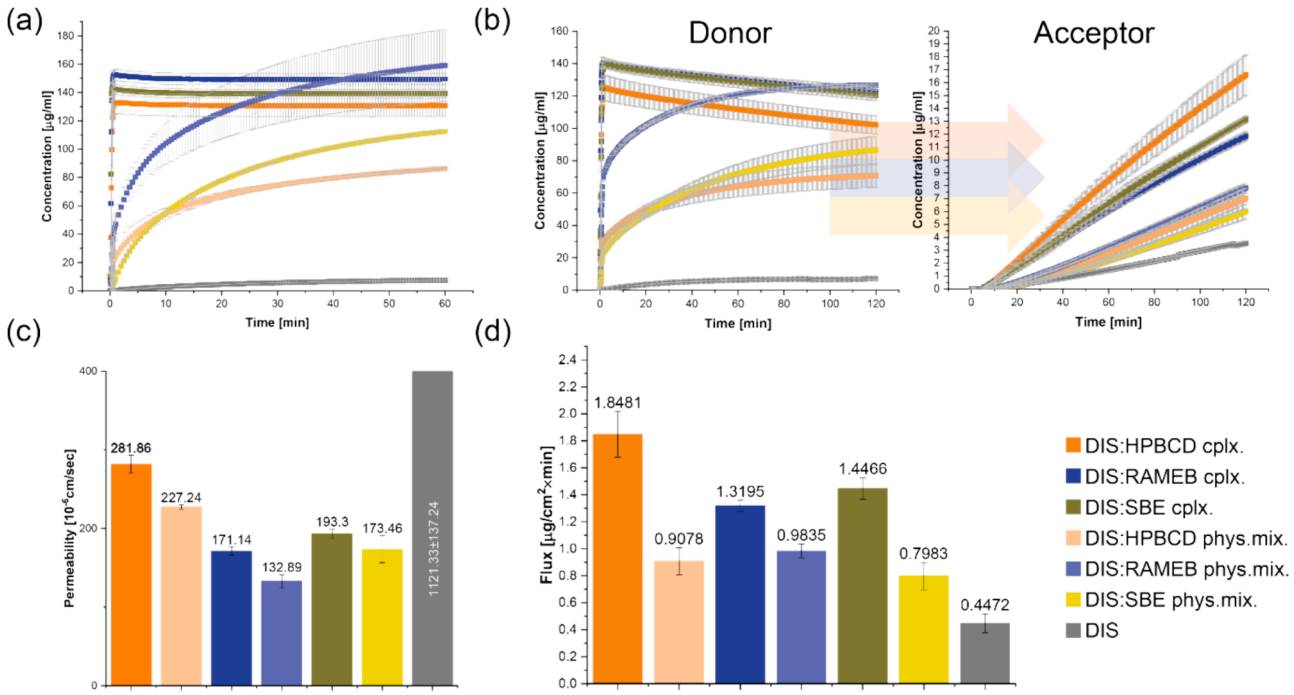

Fig. 5. The concentration of dissolved DIS in function of time, by measuring the dissolution of the prepared inclusion complexes with HPBCD, RAMEB, and SBE; the respective physical mixtures; and raw crystalline DIS powder (a). Determination of dissolution-permeation characteristics of the samples with respective concentrations on donor and acceptor sites (b): the permeability behavior (c) and flux (d) across the artificial membrane. Abbreviations: cplx. = inclusion complex of DIS with respective CD; phys.mix. = physical mixture.

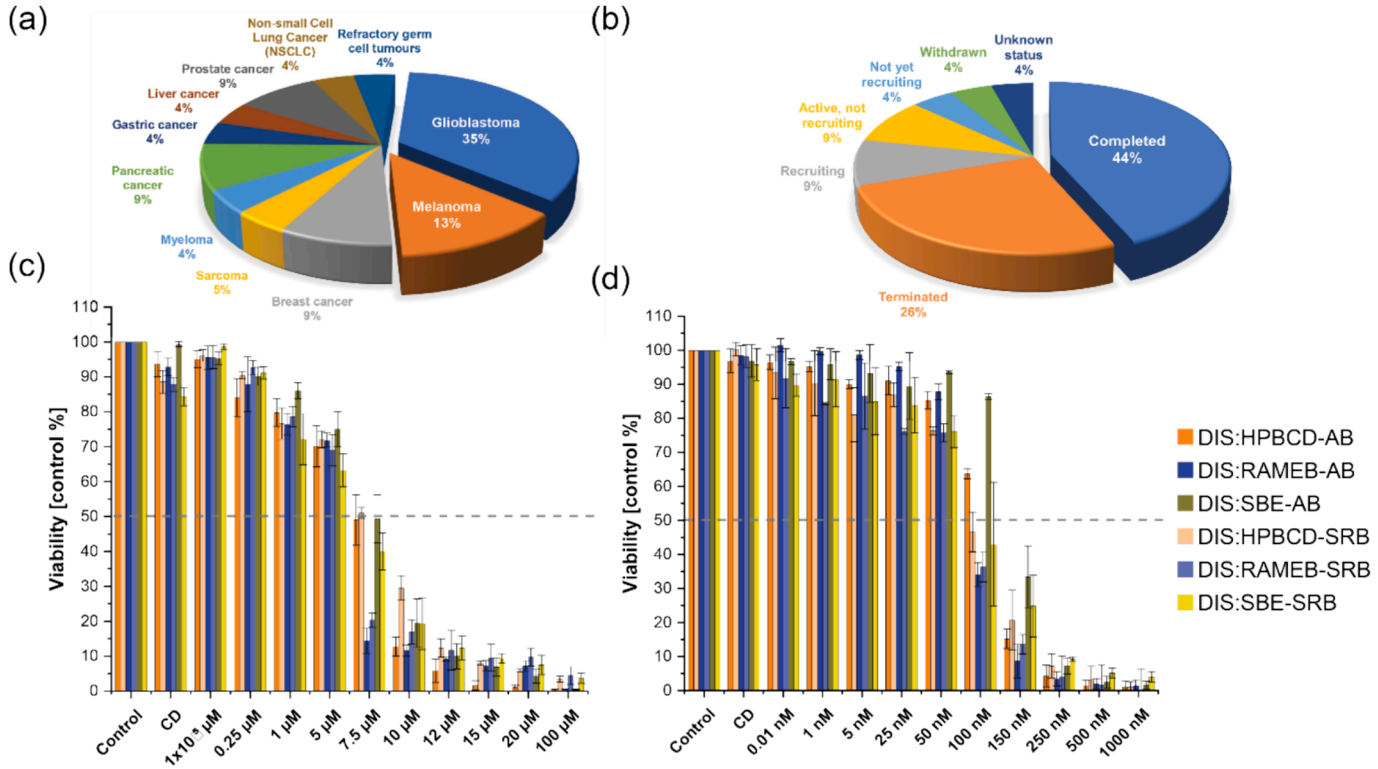

Fig. 6. The ratio of clinical trials on different tumor types (a) and completion rate (b) of the 23 registered (2023 October) clinical trials on ClinicalTrials.gov investigating DIS for cancer treatment. *In vitro* proliferation assay [using Alamar Blue (AB) and Sulforhodamine B (SRB) assays] with the inclusion complex of DIS with HPBCD, RAMEB and SBE on glioblastoma (represented by U251MG wt) (c) and melanoma (represented by A2058) (d) cell lines.

Table 2
Calculated IC_{50} (nM) values from the average proliferation-reducing effect of DIS inclusion complexes, DIS:HPBCD, DIS:RAMEB, and DIS:SBE on U251MG wt and A2058 cell lines, measured with AB and SRB assays.

	DIS:HPBCD IC_{50} [nM] ± SD		DIS:RAMEB IC_{50} [nM] ± SD		DIS:SBE IC_{50} [nM] ± SD	
	U251MG wt	*A2058*	*U251MG wt*	*A2058*	*U251MG wt*	*A2058*
AB	7062.81 ±538.47	113.41 ±3.40	6637.42 ±642.43	83.56 ±1.83	7423.18 ±518.71	136.85 ±2.74
SRB	7641.72 ±304.34	99.74 ±4.19	5807.18 ±373.84	91.84 ±16.69	6091.97 ±691.79	92.95 ± 3.09

Notes: The standard error is marked with ± symbol following the IC_{50} value.
Abbreviations: AB = Alamar Blue assay, DIS = disulfiram, HPBCD = hydroxypropyl-β-cyclodextrin, *IC50* = half-maximal inhibitory concentration, RAMEB = randomly methylated-β-cyclodextrin, SBE = sulfobutylether-β-cyclodextrin sodium salt, SD = standard deviation, SRB = Sulforhodamine B assay.

as an antiparasitic agent due to its metal-complexing effect, then for long-term treatment of alcohol dependence (Lanz et al., 2023). The biological interactions are attributed to its sulfur content, from which free thiol groups can be formed during its decomposition. These can be involved in thiocarbamate-thiol type reactions with free thiol groups of proteins and enzymes, for example, inhibiting the aldehyde dehydrogenases (ALDH); or it can form chelate complexes with metal ions (Cu^{2+}, Zn^{2+}), strongly influencing intracellular trace element-dependent processes (Allensworth et al., 2015; Benkő et al., 2023; Lanz et al., 2023; Lu et al., 2022). The anticancer activity of DIS is considered to be further potentiated by the supplementation of copper (Lu et al., 2022). DIS is a sulfur-based metal-binding compound and acts as a copper ionophore, facilitate the enhanced copper uptake in cancer cells and with the caused copper overload induces severe oxidative damage and cell apoptosis (Benkő et al., 2023; Lu et al., 2022). However, the therapeutic direction, based on DIS and copper co-mediated impairment of redox homeostasis, is debatable (Benkő et al., 2023). *In vitro* mechanistic studies on the anti-tumor effectiveness of DIS and copper have yielded enhanced cytotoxic interplay results, whereas *in vivo* is difficult to envisage the induction of apoptosis in tumor cells by a copper and DIS cocktail as the combination of DIS and copper does not have the identical molecular mechanisms to bis (diethyldithiocarbamate)-copper complex nor the simple addition effect of them (Benkő et al., 2023; Lu et al., 2022). In clinical trials, the additional copper did not significantly influence the drug's efficacy (Benkő et al., 2023). In analogy with oxidized and reduced forms of glutathione, the reduction of DIS to two moieties of DEDTC occurs readily *in vivo*, as well as *in vitro* (Gessner & Gessner, 1992). The thiol is the primary metabolite of DIS, which, in turn, can be readily oxidized to the disulfide and systems capable of bringing about this oxidation exist *in vivo* (Gessner & Gessner, 1992). The easy interconvertibility of these two agents affects their chemical and biological properties (Gessner & Gessner, 1992). To some extent the *in vivo* pharmacological activities of DIS and DEDTC overlap, suggesting that the mutual interconvertibility of these agents occurs to a pharmacologically significant extent, e.g., DIS and DEDTC both cause inhibition of acetaldehyde metabolism and chelate metals, resulting alterations in their distribution and excretion patterns (Gessner & Gessner, 1992). This is also the driving force behind the non-specific anti-cancer effects of DIS. As a multipotent molecule, DIS could affect cancer stem cell function by protein inhibition (e.g., ALDH inhibition), enhance sensitivity to radio- and chemotherapy (e.g., O-6-methylguanine-DNA methyltransferase inhibition), increase reactive oxygen species (ROS) level and modulate the tumor immune microenvironment (Lu et al., 2022). In spite of the distinguished anticancer activity, the outcome of clinical trials with the orally delivering substance is unsatisfactory, the critical failure attributed to its rapid, unwanted metabolism in the liver, leading to poor delivery efficiency to tumor tissues (Lu et al., 2022; Zhong et al., 2022). The active metabolites contribute to the alcohol-deterrent and anticancer activity of DIS however, S-methylation masks the functional thiol group and completely abolishes the antitumor processes (Kannappan et al., 2021; Lu et al., 2022). To overcome the multiple *in vivo* environment-related and drug-related barriers, nanoscale drug delivery systems have been extensively explored owing to the increase of the accumulation of DIS at the tumor site (Benkő et al., 2023; Kannappan et al., 2021; Lu et al., 2022). A classic method for molecular encapsulation is inclusion complexation with CDs, leading to improved drug solubility and concomitantly to a favorable bioavailability (Jambhekar & Breen, 2016a, 2016b).

4.2. Cyclodextrin encapsulated DIS

The complexation of DIS with HPBCD has been known for about 20 years, with the first patent in 2002 (CN1376463A) (Wang et al., 2002) describing the improvement of solubility and stability of the drug with CD for the preparation of eye drops against cataracts (Wang et al., 2004). A further characterization of inclusion complex formed by DIS and HPBCD, which can be used in the treatment of alcohol and cocaine dependence, is given by the patent WO2009083793A1 (Jacqueline et al., 2008). DIS and HPBCD complexes have been researched in the first line in ophthalmological indications (Ikebukuro et al., 2023; Wang et al., 2004), and in the last years in infectious diseases (Lyme, SARA-CoV-2) (Pereira et al., 2022; Potula et al., 2020) and oncological areas (Kaya et al., 2024; Qu et al., 2021; Said Suliman et al., 2021) together with SBE complexes (Supporting Information Table S1). Among these HPBCD complexes, for K_{stab} values, 1772 M^{-1} (Wang et al., 2004) and 1539 M^{-1} (Pereira et al., 2022) were reported, and for CE, 0.42 (Pereira et al., 2022), whereas for SBE CE = 0.64 (Pereira et al., 2022). The present comparative study, also including a new inclusion complex of DIS with RAMEB, indicates the lowest K_{stab} and CE values for HPBCD and a highest for RAMEB (Table 1). The deviation of K_{stab} values is derived from the insolubility of DIS and the sensitivity of the different instrumental methods, thus the CE is a more stable constant, comparable with literature data.

CD complexation produces several changes in the properties of the drug candidate, including enhanced solubility, physical, chemical stability, dissolution, and bioavailability (Jambhekar & Breen, 2016b). The present study confirms the impact of β-CD derivatives on the dissolution-permeation profile of a BCSII drug, DIS, with typical low water-solubility and high lipophilicity, modified by CDs. The reversed order of the samples from dissolution and permeation studies underlies the importance of the application of simultaneous dissolution-permeation analysis for the evaluation of the complexes to predict the *in vivo* behaviors (Fig. 5 a,b) (Kádár et al., 2022; Ramachandran & Sudheesh, 2021). The biorelevant donor medium selection was derived by DIS administration optimization to enhance its application in cancer therapy. The intranasal administration and nose-to-brain delivery of DIS for tackling GB is a promising administration route, bypassing the first pass effect and also the blood–brain barrier by entering through the olfactory region and reducing the unwanted metabolism of DIS (Qu et al., 2021). Similarly, the localized application is also a potential administration route for DIS; and MEL is a topically accessible cancer type (Sun et al., 2014). The dissolution-permeation results are in accordance with literature data, describing that CDs usually increase the solubility of lipophilic compounds, while also decrease the P_{eff} due to a reduction of the free drug fraction at the epithelial membrane surface and/or the reduction of the diffusion coefficient caused by the enlarged hydrodynamic radius of CD complex in contrast to the pure drug (Borbás et al., 2019; Loftsson, 2012). These effects depend also on the physicochemical properties of the drug, but as a rule, the best results with CD inclusion complexation are obtained for lipophilic drugs that are poorly soluble in water, and form water-soluble complexes with CDs and that possess, as dissolved drug molecules, relatively high permeability through lipophilic membranes (Loftsson, 2012). Therefore, the optimization of drug vehicles is

essential, as an inadequate ratio of CDs (whether too much or too little) will lead to less-than-optimal drug availability (Loftsson, 2012). An in-depth study on CD complexation and how CDs affect drug permeation through membranes is indispensable for successful CD-containing drug development (Loftsson, 2012).

The proliferation study revealed the extreme DIS sensitivity difference of U251MG wt and A2058 cell lines, being more effective on the latter one. Similarly, the literature data reflect a deviation of IC_{50} from nanoscale values to micromoles, e.g., DIS treatment reduced the viability of solid tumor cell lines (MCF-7, MDA-MB-231, HBT-3, OVCAR3 and U87) with an IC_{50} of < 0.8 μM (Nasrollahzadeh et al., 2021), the IC_{50} for GB stem cells have been reported to be in the range of 120–465 nM (Zirjacks et al., 2021), whereas for different, primary and metastatic, MEL cell lines from 38.6 ± 1.2 to 272.2 ± 71.2 nM (Morrison et al., 2010), and 2.5 μM for CRL1585 (Brar et al., 2004).

4.3. Enabling anticancer reposition of DIS by cyclodextrin encapsulation

The current therapy for GB and MEL has reached a limit of clinical responses, thus the research for alternative treatment options is a growing tendency (Lopes et al., 2022; Zhong et al., 2022). Accordingly, the clinical trials with DIS are focused on these tumor types and the selection of U251MG wt and A2058 cell lines also was guided by this. Regarding the biopharmaceutical analysis, the causes for differences seen in the line-up of the DIS inclusion complexes with the three CDs in case of dissolution/permeation prediction and proliferation assay, are multifactorial, depending on the physicochemical properties and pharmacodynamics of the drug, characteristics of the different cancer cell lines and the unique interaction of CDs with membranes.

This complexity of the mechanism of action of DIS, is thought to be well exploited against the characteristic heterogeneity of GB (Benkő et al., 2023). MEL presents particularly elevated ROS levels in comparison with other solid tumors; thus, the regulation of ROS levels is a promising therapeutic opportunity since neoplastic cells might be more sensitive to drugs that trigger further accumulation of ROS (Cannavò et al., 2019; Emanuelli et al., 2022). This could be well targeted by the interplay of DIS and its metabolite, DEDTC, generating the up-regulation of ROS and thus provoking the anti-tumor effect (Cen et al., 2004; Meraz-Torres et al., 2020).

In vitro biological experiments have shown that the decisive step in the effectiveness of DIS is the dissolution. Anti-proliferation assays suggest that despite the non-specific anti-tumor activity of the drug, there is a large variation in the sensitivity of cell lines. Within a cell line, DIS encapsulated in different CDs has a statistically similar inhibitory effect, although in both cell lines, measured by both methods, the complex with RAMEB gave a lower IC_{50}; and the physical–chemical evaluation also revealed the advantage of it. The slight difference between CD inclusion complexes may be related to their CE, solubility enhancing effect on DIS and to the CDs' selective and specific interaction with membrane components. The methylated β-CDs, such as RAMEB, has extreme affinity nearly with all types of lipid classes such as fatty acids, triglycerides, phospholipids, steroids, and carotenoids. HPBCD received the orphan drug status for the treatment of Niemann Pick type C disease, a genetic disorder of cholesterol metabolism and trafficking due to its cholesterol mobilizing effect; in contrast SBE shows very low encapsulation affinity with cholesterol, however reduces its storage (Szente & Fenyvesi, 2017).

CDs may be chosen for further pharmaceutical developments of DIS, assuming the toxicological considerations, administration routes and the unique interplay with the target environment. HPBCD and SBE are considered nontoxic when administered in low to moderate doses by oral and intravenous routes, whereas RAMEB is absorbed to a greater extent from the gastrointestinal tract into the systemic circulation and have been shown to be toxic after parenteral administration and presently also the oral administration is limited because of its potential toxicity (Jambhekar & Breen, 2016a). Recently, there are about 130 approved pharmaceutical ingredients formulated with either parent CDs or their derivatives and among these, the marketed drugs are formulated mainly with β-CD or its derivatives, such as HPBCD, SBE, and RAMEB (Puskás et al., 2023). The selectivity to remove certain lipids is governed by the cavity size and geometry of the CD nano-containers, and the produced changes in the organization of cellular membrane components can modify the basic cellular functions such as signal transduction and membrane trafficking, affecting various diseases, e.g., atherosclerosis, neurodegenerative disorders and also cancer (Okamatsu et al., 2013; Szente & Fenyvesi, 2017; Wei et al., 2023; Yokoo et al., 2015). Moreover, previously the benefit of methyl-β-CD has been described, as cholesterol depleting agent, highly sensitizing metastatic MEL cells towards tamoxifen treatment (Mohammad et al., 2014), and a recent study also revealed the role of cholesterol in glioma cell survival (Murk & Hülse, 2022).

5. Conclusions

The physicochemical and *in vitro* biological comparative analysis of the already known DIS inclusion complexes (with HPBCD and SBE) and newly synthetized (with RAMEB) reveals: the significant solubility enhancement of the drug, the fast dissolution of the lyophilized inclusion complexes and the adequate *in vitro* proliferation inhibitory activity of DIS with extreme sensitivity difference on GB and MEL cell lines. For the inclusion complexation of DIS, all three β-CD derivatives (HPBCD, SBE, RAMEB) are potential. Thus, the CD encapsulation presents a promising multivariable platform tool for anticancer repositioning of the drug. The reversed order of the inclusion complexes from the dissolution-permeation analysis and the results of the proliferation assays strengthened the importance of CD selection methodology for further drug delivery systems development, analyzing the specific interaction of CDs with the target site environment for a more effective drug administration strategy and target environment-specific anticancer repositioning of DIS. The drug's multipotential anticancer mechanism correlates with the heterogeneous tumor types; thus, its adjuvant role in cancer treatment is promising from a clinical translation perspective. Even though repurposing has become an attractive drug discovery strategy due to its cost-reducing and time-consuming efficiency, it is only partially risk-free. The new formulation (e.g., new dose, new pharmaceutical form) requires in-depth analysis of biological activity, pharmacological parameters, and clinical observations to inhibit the late-stage development phase failure. Moreover, a rational excipient selection method should be the primary goal during repositioned drug development to balance the benefits and achieve industrial scale-up, completing the healthcare assistance from bench to bedside. From this perspective, RAMEB can be a promising enabling excipient in the repositioning of DIS; their inclusion complex could serve for drug development to fulfil the unmet need, such as adjuvant local MEL therapy, also by overcoming the poor oral bioavailability of the drug.

Funding

This research was funded by the Semmelweis Science and Innovation Fund [I.S.: STIA-KFI 2022], by the New National Excellence Program of the Ministry for Culture and Innovation from the Source of the National Research, Development and Innovation Fund [B.M.B.: ÚNKP-23-3-II-SE-95 and Sz.K.: ÚNKP-23-3-II-BME-88] and supported by the National Research, Development and Innovation Office, Hungary [B.F.: TKP2021-NVA-14; G.T.: NKFIH FK 146930; A.S.: NKFI-K-142799].

CRediT authorship contribution statement

Beáta-Mária Benkő: Writing – original draft, Visualization, Software, Methodology, Investigation, Formal analysis, Data curation, Conceptualization. **Gergő Tóth:** Writing – review & editing, Methodology, Investigation, Conceptualization. **Dorottya Moldvai:** Writing – review & editing, Methodology, Investigation, Conceptualization. **Szabina Kádár:** Writing – review & editing, Methodology, Investigation,

Data curation. **Edina Szabó:** Writing – review & editing, Methodology, Investigation, Data curation. **Zoltán-István Szabó:** Writing – review & editing, Methodology, Conceptualization. **Márta Kraszni:** Writing – review & editing, Methodology, Investigation, Data curation. **Lajos Szente:** Writing – review & editing, Methodology, Conceptualization. **Béla Fiser:** Software, Investigation, Data curation. **Anna Sebestyén:** Writing – review & editing, Methodology, Investigation, Conceptualization. **Romána Zelkó:** Writing – review & editing, Methodology, Conceptualization. **István Sebe:** Writing – review & editing, Supervision, Resources, Project administration, Methodology, Funding acquisition, Conceptualization.

Declaration of competing interest

The authors declare that they have no known competing financial interests or personal relationships that could have appeared to influence the work reported in this paper.

Data availability

The authors declare that the data supporting the findings of this study are available within the paper and its supplementary information files. The datasets generated during and/or analysed during the current study are available from the corresponding author on reasonable request. Correspondence and requests for materials should be addressed to Romána Zelkó: zelko.romana@semmelweis.hu; and Beáta-Mária Benkő benko.beata@phd.semmelweis.hu.

Acknowledgements

The authors with to thank Bence Tóth (Department of Pharmaceutics, Faculty of Pharmacy, Semmelweis University, Hőgyes Endre Str. 7-9., Budapest 1092, Hungary) for the assistance in XRD measurements; Dóra Csicsák and Balázs Simon (Department of Pharmaceutical Chemistry, Semmelweis University, Hőgyes Endre Str. 7-9., Budapest 1092, Hungary) for the RAMAN and FTIR instrumental support; Titanilla Dankó and Dániel Sztankovics (Tumor Biology, Cell and Tissue Culture Laboratory, 1st Department of Pathology and Experimental Cancer Research, Semmelweis University, Üllői út 26., Budapest 1085, Hungary) for unwavering guidance in cell line culturing. The GITDA (Governmental Information-Technology Development Agency, Hungary) is gratefully acknowledged for allocating computing resources used in this work. Calculations have also been carried out using resources provided by Wroclaw Centre for Networking and Supercomputing (http://wcss.pl).

Appendix A. Supplementary material

Supplementary data to this article can be found online at https://doi.org/10.1016/j.ijpharm.2024.124187.

References

Alifieris, C., Trafalis, D.T., 2015. Glioblastoma multiforme: pathogenesis and treatment. Pharmacol. Ther. 152, 63–82. https://doi.org/10.1016/j.pharmthera.2015.05.005.

Allensworth, J.L., Evans, M.K., Bertucci, F., Aldrich, A.J., Festa, R.A., Finetti, P., Ueno, N. T., Safi, R., McDonnell, D.P., Thiele, D.J., Van Laere, S., Devi, G.R., 2015. Disulfiram (DSF) acts as a copper ionophore to induce copper-dependent oxidative stress and mediate anti-tumor efficacy in inflammatory breast cancer. Mol. Oncol. 9 (6), 1155–1168. https://doi.org/10.1016/j.molonc.2015.02.007.

Bartos, C., Szabó-Révész, P., Horváth, T., Varga, P., Ambrus, R., 2021. Comparison of modern in vitro permeability methods with the aim of investigation nasal dosage forms. Pharmaceutics 13 (6). https://doi.org/10.3390/pharmaceutics13060846.

Beneš, M., Zusková, I., Svobodová, J., Gaš, B., 2012. Determination of stability constants of complexes of neutral analytes with charged cyclodextrins by affinity capillary electrophoresis. Electrophoresis 33 (6), 1032–1039. https://doi.org/10.1002/elps.201100489.

Benkő, B.-M., Lamprou, D.A., Sebestyén, A., Zelkó, R., Sebe, I., 2023. Clinical, pharmacological and formulation evaluation of disulfiram in the treatment of glioblastoma - a systematic literature review. Expert Opin. Drug Deliv. 20 (4), 541–557. https://doi.org/10.1080/17425247.2023.2190581.

Borbás, E., Kádár, S., Tsinman, K., Tsinman, O., Csicsák, D., Takács-Novák, K., Völgyi, G., Sinkó, B., Pataki, H., 2019. Prediction of bioequivalence and food effect using flux- and solubility-based methods. Mol. Pharm. 16 (10), 4121–4130. https://doi.org/10.1021/acs.molpharmaceut.9b00406.

Brar, S.S., Grigg, C., Wilson, K.S., Holder Jr., W.D., Dreau, D., Austin, C., Foster, M., Ghio, A.J., Whorton, A.R., Stowell, G.W., Whittall, L.B., Whittle, R.R., White, D.P., Kennedy, T.P., 2004. Disulfiram inhibits activating transcription factor/cyclic AMP-responsive element binding protein and human melanoma growth in a metal-dependent manner in vitro, in mice and in a patient with metastatic disease. Mol. Cancer Ther. 3 (9), 1049–1060.

Brewster, M.E., Loftsson, T., 2007. Cyclodextrins as pharmaceutical solubilizers. Adv. Drug Deliv. Rev. 59 (7), 645–666. https://doi.org/10.1016/j.addr.2007.05.012.

Cannavò, S.P., Tonacci, A., Bertino, L., Casciaro, M., Borgia, F., Gangemi, S., 2019. The role of oxidative stress in the biology of melanoma: A systematic review. Pathology - Research and Practice 215 (1), 21–28. https://doi.org/10.1016/j.prp.2018.11.020.

Cen, D., Brayton, D., Shahandeh, B., Meyskens Jr., F.L., Farmer, P.J., 2004. Disulfiram facilitates intracellular Cu uptake and induces apoptosis in human melanoma cells. J. Med. Chem. 47 (27), 6914–6920. https://doi.org/10.1021/jm049568z.

Cheng, H.-B., Yue, W., Xie, C., Zhang, R.-Y., Hu, S.-S., Wang, Z., 2013. IDH1 mutation is associated with improved overall survival in patients with glioblastoma: a meta-analysis. Tumor Biol. 34 (6), 3555–3559. https://doi.org/10.1007/s13277-013-0934-5.

Dankó, T., Petővári, G., Sztankovics, D., Moldvai, D., Raffay, R., Lőrincz, P., Visnovitz, T., Zsiros, V., Barna, G., Márk, Á., Krencz, I., Sebestyén, A., 2021. Rapamycin plus doxycycline combination affects growth arrest and selective autophagy-dependent cell death in breast cancer cells. Int. J. Mol. Sci. 22 (15) https://doi.org/10.3390/ijms22158019.

Dhiman, P., Bhatia, M., 2020. Pharmaceutical applications of cyclodextrins and their derivatives. J. Incl. Phenom. Macrocycl. Chem. 98 (3), 171–186. https://doi.org/10.1007/s10847-020-01029-3.

Emanuelli, M., Sartini, D., Molinelli, E., Campagna, R., Pozzi, V., Salvolini, E., Simonetti, O., Campanati, A., Offidani, A., 2022. The double-edged sword of oxidative stress in skin damage and melanoma: From physiopathology to therapeutical approaches. Antioxidants (Basel) 11 (4). https://doi.org/10.3390/antiox11040612.

Farooq, M.A., Aquib, M., Khan, D.H., Hussain, Z., Ahsan, A., Baig, M.M.F.A., Wande, D. P., Ahmad, M.M., Ahsan, H.M., Jiajie, J., Wang, B., 2019. Recent advances in the delivery of disulfiram: a critical analysis of promising approaches to improve its pharmacokinetic profile and anticancer efficacy. DARU J. Pharmaceut. Sci. 27 (2), 853–862. https://doi.org/10.1007/s40199-019-00308-w.

Gampa, G., Vaidhyanathan, S., Sarkaria, J.N., Elmquist, W.F., 2017. Drug delivery to melanoma brain metastases: Can current challenges lead to new opportunities? Pharmacol. Res. 123, 10–25. https://doi.org/10.1016/j.phrs.2017.06.008.

Gessner, P.K., Gessner, T., 1992. Introduction and scope of monograph. In: Gessner, P.K., Gessner, T. (Eds.), Disulfiram and its metabolite, diethyldithiocarbamate: pharmacology and status in the treatment of alcoholism, HIV infections, AIDS and heavy metal toxicity (pp. 1-6). Springer Netherlands. doi: 10.1007/978-94-011-2328-0_1.

Halatsch, M.E., Kast, R.E., Karpel-Massler, G., Mayer, B., Zolk, O., Schmitz, B., Scheuerle, A., Maier, L., Bullinger, L., Mayer-Steinacker, R., Schmidt, C., Zeiler, K., Elshaer, Z., Panther, P., Schmelzle, B., Hallmen, A., Dwucet, A., Siegelin, M. D., Westhoff, M.A., Heiland, T., 2021. A phase Ib/IIa trial of 9 repurposed drugs combined with temozolomide for the treatment of recurrent glioblastoma: CUSP9v3. Neuro-Oncol. Adv. 3(1), vdab075, Article vdab075. doi: 10.1093/noajnl/vdab075.

Hetényi, C., van der Spoel, D., 2002. Efficient docking of peptides to proteins without prior knowledge of the binding site. Protein Sci. 11 (7), 1729–1737. https://doi.org/10.1110/ps.0202302.

Higuchi, T., Connor, K.A., 1965. Phase solubility techniques (New York).

Hua, Y., Dai, X., Xu, Y., Xing, G., Liu, H., Lu, T., Chen, Y., Zhang, Y., 2022. Drug repositioning: progress and challenges in drug discovery for various diseases. Eur. J. Med. Chem. 234, 114239 https://doi.org/10.1016/j.ejmech.2022.114239.

Huang, J.Y., Campian, J.L., Gujar, A.D., Tran, D.D., Lockhart, A.C., DeWees, T.A., Tsien, C.I., Kim, A.H., 2016. A phase I study to repurpose disulfiram in combination with temozolomide to treat newly diagnosed glioblastoma after chemoradiotherapy. J. Neurooncol 128 (2), 259–266. https://doi.org/10.1007/s11060-016-2104-2.

Huang, J.Y., Campian, J.L., Gujar, A.D., Tsien, C., Ansstas, G., Tran, D.D., DeWees, T.A., Lockhart, A.C., Kim, A.H., 2018. Final results of a phase I dose-escalation, dose-expansion study of adding disulfiram with or without copper to adjuvant temozolomide for newly diagnosed glioblastoma. J. Neurooncol 138 (1), 105–111. https://doi.org/10.1007/s11060-018-2775-y.

Huang, J.Y., Chaudhary, R., Cohen, A.L., Fink, K., Goldlust, S., Boockvar, J., Chinnaiyan, P., Wan, L.P., Marcus, S., Campian, J.L., 2019. A multicenter phase II study of temozolomide plus disulfiram and copper for recurrent temozolomide-resistant glioblastoma. J. Neurooncol 142 (3), 537–544. https://doi.org/10.1007/s11060-019-03125-y.

Hujber, Z., Horváth, G., Petővári, G., Krencz, I., Dankó, T., Mészáros, K., Rajnai, H., Szoboszlai, N., Leenders, W.P.J., Jeney, A., Tretter, L., Sebestyén, A., 2018. GABA, glutamine, glutamate oxidation and succinic semialdehyde dehydrogenase expression in human gliomas. J. Exp. Clin. Can. Res. 37 (1), 271. https://doi.org/10.1186/s13046-018-0946-5.

Ichimura, K., Pearson, D.M., Kocialkowski, S., Bäcklund, L.M., Chan, R., Jones, D.T.W., Collins, V.P., 2009. IDH1 mutations are present in the majority of common adult gliomas but rare in primary glioblastomas. Neuro Oncol. 11 (4), 341–347. https://doi.org/10.1215/15228517-2009-025.

Ikebukuro, T., Arima, T., Kasamatsu, M., Nakano, Y., Tobita, Y., Uchiyama, M., Terashima, Y., Toda, E., Shimizu, A., Takahashi, H., 2023. Disulfiram ophthalmic solution inhibited macrophage infiltration by suppressing macrophage pseudopodia formation in a rat corneal alkali burn model. Int. J. Mol. Sci. 24 (1) https://doi.org/10.3390/ijms24010735.

Jacqueline, M., Carreño, S., Guillermo Von Plessing, C., Edson, R., Montero Cabrera F., 2008. Universidad De Concepcion, Laboratorios Andromaco S.A., Abl Pharma Colombia S.A. WO2009083793A1.

Jambhekar, S.S., Breen, P., 2016a. Cyclodextrins in pharmaceutical formulations I: structure and physicochemical properties, formation of complexes, and types of complex. Drug Discov. Today 21 (2), 356–362. https://doi.org/10.1016/j.drudis.2015.11.017.

Jambhekar, S.S., Breen, P., 2016b. Cyclodextrins in pharmaceutical formulations II: solubilization, binding constant, and complexation efficiency. Drug Discov. Today 21 (2), 363–368. https://doi.org/10.1016/j.drudis.2015.11.016.

Jullian, C., Morales-Montecinos, J., Zapata-Torres, G., Aguilera, B., Rodriguez, J., Arán, V., Olea-Azar, C., 2008. Characterization, phase-solubility, and molecular modeling of inclusion complex of 5-nitroindazole derivative with cyclodextrins. Bioorg. Med. Chem. 16 (9), 5078–5084. https://doi.org/10.1016/j.bmc.2008.03.026.

Kádár, S., Tőzsér, P., Nagy, B., Farkas, A., Nagy, Z.K., Tsinman, O., Tsinman, K., Csicsák, D., Völgyi, G., Takács-Novák, K., Borbás, E., Sinkó, B., 2022. Flux-based formulation development—a proof of concept study. AAPS J. 24 (1), 22. https://doi.org/10.1208/s12248-021-00668-9.

Kang, J.S., Hwang, S., Lee, C.-J., Lee, M.-S., 2002. SERS of dithiocarbamate pesticides adsorbed on silver surface; Thiram. Bull. Kor. Chem. Soc. 23, 1604–1610.

Kannappan, V., Ali, M., Small, B., Rajendran, G., Elzhenni, S., Taj, H., Wang, W., Dou, Q. P., 2021. Recent advances in repurposing disulfiram and disulfiram derivatives as copper-dependent anticancer agents. Front. Mol. Biosci. 8, 741316 https://doi.org/10.3389/fmolb.2021.741316.

Kaya, A., Arafat, B., Chichger, H., Tolaymat, I., Pierscionek, B., Khoder, M., Najlah, M., 2024. Preparation and characterisation of zinc diethyldithiocarbamate-cyclodextrin inclusion complexes for potential lung cancer treatment. Pharmaceutics 16 (1), 65. https://doi.org/10.3390/pharmaceutics16010065.

Kelley, K.C., Grossman, K.F., Brittain-Blankenship, M., Thorne, K.M., Akerley, W.L., Terrazas, M.C., Kosak, K.M., Boucher, K.M., Buys, S.S., McGregor, K.A., Werner, T.L., Agarwal, N., Weis, J.R., Sharma, S., Ward, J.H., Kennedy, T.P., Sborov, D.W., Shami, P.J., 2021. A Phase 1 dose-escalation study of disulfiram and copper gluconate in patients with advanced solid tumors involving the liver using S-glutathionylation as a biomarker. BMC Cancer 21 (1), 510. https://doi.org/10.1186/s12885-021-08242-4.

Lanz, J., Biniaz-Harris, N., Kuvaldina, M., Jain, S., Lewis, K., Fallon, B.A., 2023. Disulfiram: mechanisms, applications, and challenges. Antibiotics 12 (3). https://doi.org/10.3390/antibiotics12030524.

Loftsson, T., 2012. Drug permeation through biomembranes: cyclodextrins and the unstirred water layer. Die Pharmazie - An Int. J. Pharmaceut. Sci. 67 (5), 363–370. https://doi.org/10.1691/ph.2012.1698.

Loftsson, T., Hreinsdóttir, D., Másson, M., 2005. Evaluation of cyclodextrin solubilization of drugs. Int. J. Pharm. 302 (1), 18–28. https://doi.org/10.1016/j.ijpharm.2005.05.042.

Lopes, J., Rodrigues, C.M.P., Gaspar, M.M., Reis, C.P., 2022. Melanoma management: From epidemiology to treatment and latest advances. Cancers 14 (19).

Lu, C., Li, X., Ren, Y., Zhang, X., 2021. Disulfiram: a novel repurposed drug for cancer therapy. Can. Chemother. Pharmacol. 87 (2), 159–172. https://doi.org/10.1007/s00280-020-04216-8.

Lu, Y., Pan, Q., Gao, W., Pu, Y., Luo, K., He, B., Gu, Z., 2022. Leveraging disulfiram to treat cancer: Mechanisms of action, delivery strategies, and treatment regimens. Biomaterials 281, 121335. https://doi.org/10.1016/j.biomaterials.2021.121335.

Mego, M., Svetlovska, D., Angelis V, D., Kalavska, K., Lesko, P., Makovník, M., Obertova, J., Orszaghova, Z., Palacka, P., Rečková, M., Rejlekova, K., Z, S.-M., Mardiak, J., Chovanec, M., 2022. Phase II study of disulfiram and cisplatin in refractory germ cell tumors. The GCT-SK-006 phase II trial. Investigational New Drugs, 40(5), 1080-1086. doi: 10.1007/s10637-022-01271-1.

Meraz-Torres, F., Plöger, S., Garbe, C., Niessner, H., Sinnberg, T., 2020. Disulfiram as a therapeutic agent for metastatic malignant melanoma—Old myth or new logos? Cancers 12 (12). https://doi.org/10.3390/cancers12123538.

Mohammad, N., Malvi, P., Meena, A.S., Singh, S.V., Chaube, B., Vannuruswamy, G., Kulkarni, M.J., Bhat, M.K., 2014. Cholesterol depletion by methyl-β-cyclodextrin augments tamoxifen induced cell death by enhancing its uptake in melanoma. Mol. Can. 13 (1), 204. https://doi.org/10.1186/1476-4598-13-204.

Morrison, B.W., Doudican, N.A., Patel, K.R., Orlow, S.J., 2010. Disulfiram induces copper-dependent stimulation of reactive oxygen species and activation of the extrinsic apoptotic pathway in melanoma. Melanoma Res. 20 (1) https://doi.org/10.1097/CMR.0b013e328334131d.

Murk, K., Hülse, R., 2022. Forced but effective partners in crime: how astrocytes drive the progression of glioblastoma. Brain 145 (9), 2952–2954. https://doi.org/10.1093/brain/awac302.

Nasrollahzadeh, A., Momeny, M., Fasehee, H., Yaghmaie, M., Bashash, D., Hassani, S., Mousavi, S.A., Ghaffari, S.H., 2021. Anti-proliferative activity of disulfiram through regulation of the AKT-FOXO axis: A proteomic study of molecular targets. Biochimica et Biophysica Acta (BBA) - Molecular. Cell Res. 1868 (10), 119087 https://doi.org/10.1016/j.bbamcr.2021.119087.

Nechushtan, H., Hamamreh, Y., Nidal, S., Gotfried, M., Baron, A., Shalev, Y.I., Nisman, B., Peretz, T., Peylan-Ramu, N., 2015. A phase IIb trial assessing the addition of disulfiram to chemotherapy for the treatment of metastatic non-small cell lung cancer. Oncologist 20 (4), 366–367. https://doi.org/10.1634/theoncologist.2014-0424.

Okamatsu, A., Motoyama, K., Onodera, R., Higashi, T., Koshigoe, T., Shimada, Y., Hattori, K., Takeuchi, T., Arima, H., 2013. Folate-appended β-cyclodextrin as a promising tumor targeting carrier for antitumor drugs in vitro and in vivo. Bioconjug. Chem. 24 (4), 724–733. https://doi.org/10.1021/bc400015r.

Pereira, A.M., Kaya, A., Alves, D., Ansari-Fard, N., Tolaymat, I., Arafat, B., Najlah, M., 2022. Preparation and characterization of disulfiram and beta cyclodextrin inclusion complexes for potential application in the treatment of SARS-CoV-2 via nebulization. Molecules 27 (17), 5600. https://doi.org/10.3390/molecules27175600.

Potula, H.S.K., Shahryari, J., Inayathullah, M., Malkovskiy, A.V., Kim, K.M., Rajadas, J., 2020. Repurposing disulfiram (tetraethylthiuram disulfide) as a potential drug candidate against Borrelia burgdorferi in vitro and in vivo. Antibiotics (basel) 9 (9). https://doi.org/10.3390/antibiotics9090633.

Pu, H., Huang, Z., Xu, F., Sun, D.-W., 2021. Two-dimensional self-assembled Au-Ag core-shell nanorods nanoarray for sensitive detection of thiram in apple using surface-enhanced Raman spectroscopy. Food Chem. 343, 128548 https://doi.org/10.1016/j.foodchem.2020.128548.

Puskás, I., Szente, L., Szőcs, L., Fenyvesi, É., 2023. Recent list of cyclodextrin-containing drug products. Period. Polytech., Chem. Eng. 67 (1), 11–17. https://doi.org/10.3311/ppch.21222.

Qu, Y., Sun, X., Ma, L., Li, C., Xu, Z., Ma, W., Zhou, Y., Zhao, Z., Ma, D., 2021. Therapeutic effect of disulfiram inclusion complex embedded in hydroxypropyl-β-cyclodextrin on intracranial glioma-bearing male rats via intranasal route. Eur. J. Pharm. Sci. 156, 105590 https://doi.org/10.1016/j.ejps.2020.105590.

Ramachandran, G., Sudheesh, M.S., 2021. Role of permeability on the biopredictive dissolution of amorphous solid dispersions. AAPS PharmSciTech 22 (7), 243. https://doi.org/10.1208/s12249-021-02125-4.

Ramadhani, N., Shabir, M., McConville, C., 2014. Preparation and characterisation of Kolliphor® P 188 and P 237 solid dispersion oral tablets containing the poorly water soluble drug disulfiram. Int. J. Pharm. 475 (1), 514–522. https://doi.org/10.1016/j.ijpharm.2014.09.013.

Said Suliman, A., Khoder, M., Tolaymat, I., Webster, M., Alany, R.G., Wang, W., Elhissi, A., Najlah, M., 2021. Cyclodextrin diethyldithiocarbamate copper II inclusion complexes: A promising chemotherapeutic delivery system against chemoresistant triple negative breast cancer cell lines. Pharmaceutics 13 (1). https://doi.org/10.3390/pharmaceutics13010084.

Saokham, P., Muankaew, C., Jansook, P., Loftsson, T., 2018. Solubility of cyclodextrins and drug/cyclodextrin complexes. Molecules 23 (5), 1161. https://doi.org/10.3390/molecules23051161.

Schweizer, M.T., Bardia, A., Blackford, A.L., Lin, J., Armstrong, A.J., King, S., Rudek, M. A., Yegnasubramanian, S.T., Carducci, M.A., 2013. A prostate cancer clinical trials consortium trial of disulfiram (D) in men with nonmetastatic recurrent prostate cancer (PCa). J. Clin. Oncol. 31 (6_suppl), 219. https://doi.org/10.1200/jco.2013.31.6_suppl.219.

Sid, D., Baitiche, M., Elbahri, Z., Djerboua, F., Boutahala, M., Bouaziz, Z., Le Borgne, M., 2021. Solubility enhancement of mefenamic acid by inclusion complex with β-cyclodextrin: in silico modelling, formulation, characterisation, and in vitro studies. J. Enzyme Inhib. Med. Chem. 36 (1), 605–617. https://doi.org/10.1080/14756366.2020.1869225.

Sravani, A.B., Shenoy K.M., Chandrika, B., Kumar B.H., Kini, S.G., Pai K.S.R., Lewis, S.A., 2023. Curcumin-sulfobutyl-ether beta cyclodextrin inclusion complex: preparation, spectral characterization, molecular modeling, and antimicrobial activity. J. Biomol. Struct. Dyn. 1–16. doi: 10.1080/07391102.2023.2254409.

Sun, Y., Du, L., Liu, Y., Li, X., Li, M., Jin, Y., Qian, X., 2014. Transdermal delivery of the in situ hydrogels of curcumin and its inclusion complexes of hydroxypropyl-β-cyclodextrin for melanoma treatment. Int. J. Pharm. 469 (1), 31–39. https://doi.org/10.1016/j.ijpharm.2014.04.039.

Szabó, Z.-I., Orbán, G., Borbás, E., Csicsák, D., Kádár, S., Fiser, B., Dobó, M., Horváth, P., Kiss, E., Budai, L., Dobos, J., Pálla, T., Őrfi, L., Völgyi, G., Tóth, G., 2021. Inclusion complexation of the anticancer drug pomalidomide with cyclodextrins: fast dissolution and improved solubility. Heliyon 7 (7), e07581.

Szente, L., Fenyvesi, É., 2017. Cyclodextrin-lipid complexes: Cavity size matters. Struct. Chem. 28 (2), 479–492. https://doi.org/10.1007/s11224-016-0884-9.

Thordarson, P., 2011. Determining association constants from titration experiments in supramolecular chemistry. Chem. Soc. Rev. 40 (3), 1305–1323. https://doi.org/10.1039/C0CS00062K.

Tóth, G., Jánoska, Á., Völgyi, G., Szabó, Z.-I., Orgován, G., Mirzahosseini, A., Noszál, B., 2017. Physicochemical characterization and cyclodextrin complexation of the anticancer drug lapatinib. J. Chem. 2017, 4537632. https://doi.org/10.1155/2017/4537632.

Trott, O., Olson, A.J., 2010. AutoDock Vina: Improving the speed and accuracy of docking with a new scoring function, efficient optimization, and multithreading. J. Comput. Chem. 31 (2), 455–461. https://doi.org/10.1002/jcc.21334.

Tyukova, V.S., Kedik, S.A., Panov, A.V., Zhavoronok, E.S., Zolotareva, M.S., 2016. Preparation and molecular composition of an inclusion complex of dilsulfiram and hydroxypropyl-β-cyclodextrin. Pharm. Chem. J. 50 (1), 38–43. https://doi.org/10.1007/s11094-016-1395-0.

Tyukova, V.S., Kedik, S.A., Panov, A.V., Zhavoronok, E.S., Mendeleev, D.I., Senchikhin, I. N., Fursova, A.Z., Rumyantseva, Y.V., Kolosova, N.G., 2020. Synthesis of a disulfuram inclusion complex with hydroxypropyl-β-cyclodextrin and its effect on cataract development in rats. Pharm. Chem. J. 53 (12), 1158–1163. https://doi.org/10.1007/s11094-020-02140-y.

Wang, S., Li, D., Wang, S., Zhang, J., Wu, C., & Ito, Y. (2002, Shenyang Pharmaceutical University) CN1376463A.

Ulatowski, F., Dąbrowa, K., Bałakier, T., Jurczak, J., 2016. Recognizing the limited applicability of job plots in studying host–guest interactions in supramolecular chemistry. J. Org. Chem. 81 (5), 1746–1756. https://doi.org/10.1021/acs.joc.5b02909.

Wang, S., Li, D., Ito, Y., Nabekura, T., Wang, S., Zhang, J., Wu, C., 2004. Bioavailability and anticataract effects of a topical ocular drug delivery system containing disulfiram and hydroxypropyl-beta-cyclodextrin on selenite-treated rats. Curr. Eye Res. 29 (1), 51–58. https://doi.org/10.1080/02713680490513209.

Wei, X., Yu, C.-Y., Wei, H., 2023. Application of Cyclodextrin for Cancer Immunotherapy. Molecules 28 (14). https://doi.org/10.3390/molecules28145610.

Werlenius, K., Kinhult, S., Solheim, T.S., Magelssen, H., Löfgren, D., Mudaisi, M., Hylin, S., Bartek Jr., J., Strandéus, M., Lindskog, M., Rashid, H.B., Carstam, L., Gulati, S., Solheim, O., Bartek, J., Salvesen, Ø., Jakola, A.S., 2023. Effect of disulfiram and copper plus chemotherapy vs chemotherapy alone on survival in patients with recurrent glioblastoma: a randomized clinical trial. JAMA Netw. Open 6 (3), e234149–e. https://doi.org/10.1001/jamanetworkopen.2023.4149.

Wieder, R., Adam, N., 2022. Drug repositioning for cancer in the era of AI, big omics, and real-world data. Crit. Rev. Oncol. Hematol. 175, 103730 https://doi.org/10.1016/j.critrevonc.2022.103730.

Würth, R., Thellung, S., Bajetto, A., Mazzanti, M., Florio, T., Barbieri, F., 2016. Drug-repositioning opportunities for cancer therapy: novel molecular targets for known compounds. Drug Discov. Today 21 (1), 190–199. https://doi.org/10.1016/j.drudis.2015.09.017.

Yokoo, M., Kubota, Y., Motoyama, K., Higashi, T., Taniyoshi, M., Tokumaru, H., Nishiyama, R., Tabe, Y., Mochinaga, S., Sato, A., Sueoka-Aragane, N., Sueoka, E., Arima, H., Irie, T., Kimura, S., 2015. 2-hydroxypropyl-β-cyclodextrin acts as a novel anticancer agent. PLoS One 10 (11), e0141946.

Zhang, C., Xu, T., Zhang, D., He, W., Wang, S., Jiang, T., 2018. Disulfiram thermosensitive in-situ gel based on solid dispersion for cataract. Asian J. Pharm. Sci. 13 (6), 527–535. https://doi.org/10.1016/j.ajps.2018.02.010.

Zhao, P., Tang, X., Huang, Y., 2021. Teaching new tricks to old dogs: A review of drug repositioning of disulfiram for cancer nanomedicine. VIEW 2 (4), 20200127. https://doi.org/10.1002/VIW.20200127.

Zhong, S., Shengyu, L., Xin, S., Zhang, X., Li, K., Liu, G., Li, L., Tao, S., Zheng, B., Sheng, W., Ye, Z., Xing, Q., Zhai, Q., Ren, L., Wu, Y., Bao, Y., 2022. Disulfiram in glioma: Literature review of drug repurposing. Front. Pharmacol. 13, 933655 https://doi.org/10.3389/fphar.2022.933655.

Zirjacks, L., Stransky, N., Klumpp, L., Prause, L., Eckert, F., Zips, D., Schleicher, S., Handgretinger, R., Huber, S.M., Ganser, K., 2021. Repurposing disulfiram for targeting of glioblastoma stem cells: an in vitro study. Biomolecules 11 (11). https://doi.org/10.3390/biom11111561.